

A Stochastic ADMM Algorithm for Large-Scale Ptychography with Weighted Difference of Anisotropic and Isotropic Total Variation*

Kevin Bui[†] and Zichao (Wendy) Di[‡]

Abstract. Ptychography is an imaging technique that has various scientific applications, ranging from biology to optics. The method scans the object of interest in a series of overlapping positions, thereby generating a set of multiple Fourier magnitude measurements that are potentially corrupted by noise. From these measurements, an image of the object can be reconstructed depending on how the related inverse problem is formulated and solved. In this paper, we propose a class of variational models that incorporate the weighted anisotropic–isotropic total variation (AITV), an effective regularizer for image recovery. This class of models is applicable to measurements corrupted by either Gaussian or Poisson noise. In order to have the models applicable for large number of ptychographic scans, we design an efficient stochastic alternating direction method of multipliers algorithm and establish its convergence. Numerical experiments demonstrate that from a large set of highly corrupted Fourier measurements, the proposed stochastic algorithm with AITV regularization can reconstruct complex-valued images with satisfactory quality, especially for the phase components.

AMS subject classifications. 65F22, 65K10, 68U10, 90C06, 90C15, 90C26

Key words. phase retrieval, total variation, ptychography, ADMM, Poisson/Gaussian noise, nonconvex optimization, stochastic optimization

1. Introduction. Ptychography is a popular imaging technique that combines both coherent diffractive imaging and scanning transmission microscopy. It has been used in various industrial and scientific applications, including biology [34, 45, 58], crystallography [14], and optics [44, 48]. To perform a ptychographic experiment (see Figure 1), a coherent beam is scanned across the object of interest, where each scan may have overlapping positions with another. The scanning procedure provides a set of phaseless measurements that can be used to reconstruct an image of the object of interest.

We describe the 2D ptychography in the discrete setting. Let $z \in \mathbb{C}^{n^2}$ be the object of interest with $n \times n$ pixels and $\omega \in \mathbb{C}^{m^2}$ be the localized 2D probe with $m \times m$ pixels, where $m < n$. Both the object z and the probe ω are expressed as vectors in lexicographical order. We denote the set of N masks by $\{S_j\}_{j=1}^N$, where each $S_j \in \mathbb{R}^{m^2 \times n^2}$ is a binary matrix that represents a $(m \times m)$ -size window over the image z . The set of phaseless measurements $\{d_j\}_{j=1}^N$ is obtained by $d_j = |\mathcal{F}(P_j z)|^2 = |\mathcal{F}(\omega \circ S_j z)|^2$, where $P_j := \omega \circ S_j$ is the j th probe, $\mathcal{F} \in \mathbb{C}^{m^2 \times m^2}$ is the 2D discrete Fourier operator, the operation \circ is elementwise multiplication, and the operation $|\cdot|$ is the elementwise absolute value of a vector. We aim to solve the following ptychographic phase retrieval problems. When the probe is unknown, the blind ptychographic

*Submitted to the editors DATE.

Funding: This material is based upon work supported by the U.S. Department of Energy, Office of Science, under contract number DE-AC02-06CH11357.

[†]Department of Mathematics, University of California at Irvine, Irvine, CA 92697 USA (kevinb3@uci.edu).

[‡]Mathematics and Computer Science Division, Argonne National Laboratory, Lemont, IL (wendydi@anl.gov).

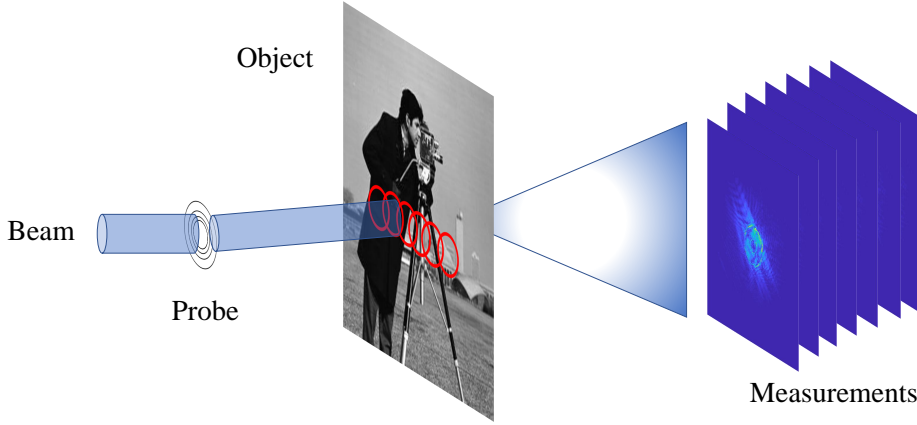


Figure 1: Schematic of a ptychography experiment.

phase retrieval problem is expressed by

(1.1)

BP-PR: To find $\omega \in \mathbb{C}^{m^2}$ and $z \in \mathbb{C}^{n^2}$ such that $|\mathcal{F}(\omega \circ S_j z)|^2 = d_j$, $j = 1, \dots, N$.

When the probe ω is known, (1.1) reduces to the non-blind case where we only find $z \in \mathbb{C}^{n^2}$.

Multiple algorithms have been developed to solve the non-blind and blind phase retrieval problems. One of the most popular methods is the ptychographical iterative engine (PIE) [42], where later refinements led to ePIE [33] and rPIE [32]. The PIE methods are based on gradient descent applied to each measurement sequentially. Other gradient-based methods for phase retrieval include Wirtinger flow [6] and its variants [13, 56, 57], which use careful initialization by a spectral method and adaptive step sizes. PIE is also one class of projection algorithms for phase retrieval. Other projection-based algorithms are hybrid projection-reflection [1], Douglas-Rachford splitting [39, 46], and the relaxed averaged alternating reflections [31]. The phase retrieval problem can be formulated as a semidefinite optimization problem. For example, PhaseLift [7] solves the phase retrieval problem as a trace (nuclear) norm minimization problem. A nonconvex variant called PhaseLiftOff subtracts the trace norm by the Frobenius norm in the objective function [55]. PhaseCut proposes a different semidefinite formulation of the phase retrieval problem by explicitly separating the amplitude and phase variables and optimize only the values of the phase variables [47]. The phase retrieval problem can alternatively be written as a saddle point problem [51], solved by alternating direction method of multipliers (ADMM) [4]. A globally convergent ADMM algorithm has recently been developed to solve the BP-PR problem [8]. Another globally convergent algorithm is proximal alternating linearized minimization (PALM) [2], which has also been adapted to solve the BP-PR problem [12, 21]. For a detailed survey of numerical algorithms for phase retrieval, please refer to [17].

For large-scale ptychography, when a huge number of scans are collected, many of the aforementioned algorithms may be inapplicable or may need to be adapted because of the

demanding memory footprint and computational cost. Various parallel algorithms have been developed. For example, an asynchronous parallel version of ePIE has been implemented on GPUs, where each partition of a measurement set is asynchronously processed to obtain a sub-image and the sub-images are later fused together to form the entire image [35]. A parallel version of relaxed averaged alternating reflections has recently been developed for GPU implementation [15]. Unfortunately, some of these parallel algorithms require a GPU, which many computers do not have. However, there are efficient algorithms for large-scale ptychography without the need for a GPU, although having one could speed up the processing time. A multigrid optimization framework has been proposed to accelerate large-scale gradient-based methods for phase retrieval [52]. An overlapping domain decomposition method combined with ADMM leads to a highly parallel algorithm with good load balance [9]. To the best of our knowledge, there does not yet exist a stochastic optimization algorithm for large-scale ptychography that iteratively processes a batch of measurements. Such an algorithm would be useful for practitioners who do not have access to multiple cores to perform parallel computing.

To improve the image reconstruction quality in phase retrieval, total variation (TV) [43] has been incorporated for the cases when the measurements are corrupted with Gaussian noise [11] or with Poisson noise [10]. Both cases consider the isotropic TV approximation:

$$(1.2) \quad \|\nabla z\|_{2,1} = \sum_{i=1}^{n^2} \sqrt{|(\nabla_x z)_i|^2 + |(\nabla_y z)_i|^2},$$

where ∇_x and ∇_y are the horizontal and vertical difference operators, respectively, and $(\nabla_x z)_i$ and $(\nabla_y z)_i$ are the i th entries of the vectors $\nabla_x z$ and $\nabla_y z$, respectively. However, it has been known that isotropic TV tends to blur oblique edges. An alternative approximation that preserves sharper edges is the anisotropic TV [16]:

$$(1.3) \quad \|\nabla z\|_1 = \sum_{i=1}^{n^2} (|(\nabla_x z)_i| + |(\nabla_y z)_i|).$$

Overall, TV is meant to approximate the ℓ_0 “norm” of the image gradient, i.e., $\|\nabla z\|_0$, because TV is based on the ℓ_1 norm, a convex relaxation of ℓ_0 . A nonconvex alternative to ℓ_1 is $\ell_1 - \alpha\ell_2$, $0 < \alpha \leq 1$, which performs well in recovering sparse solutions in various compressed sensing problems [27, 28, 29, 54]. The superior performance of $\ell_1 - \alpha\ell_2$ in sparse recovery has motivated the development of the weighted difference of anisotropic and isotropic total variation (AITV) [30], which applies $\ell_1 - \alpha\ell_2$ on each gradient vector of an image. Mathematically, AITV is formulated by

$$(1.4) \quad \|\nabla z\|_1 - \alpha\|\nabla z\|_{2,1} = \sum_{i=1}^{n^2} \left[|(\nabla_x z)_i| + |(\nabla_y z)_i| - \alpha\sqrt{|(\nabla_x z)_i|^2 + |(\nabla_y z)_i|^2} \right].$$

AITV has demonstrated better performance than TV in image denoising, image deconvolution, image segmentation, and MRI reconstruction [5, 30, 38], especially in preserving sharper edges.

In this work, we consider the large-scale ptychography problem where the measurements are corrupted by either Gaussian or Poisson noise. To improve the image reconstruction

quality, the AITV regularization is incorporated. The overall problem is formulated as a general variational problem, where we develop an ADMM algorithm to solve it. The ADMM algorithm has subproblems that can be approximately solved by stochastic gradient descent (SGD) [40]. Although SGD is a generic and popular algorithm for unconstrained optimization problems whose objective functions have a finite-sum structure, it may not be directly applicable to the subproblem being solved in the case of ptychography. Hence, we show how to appropriately apply SGD in order to develop our specialized stochastic ADMM algorithm. To further modify the algorithm, we incorporate adaptive step size based on the PIE algorithms [32, 33, 42]. Instead of using all measurements per iteration, this stochastic ADMM algorithm can iteratively process a batch of measurements to accurately perform image reconstruction.

The paper is organized as follows. In Section 2, we review notations and definitions that will be used throughout the paper. Next in Section 3 we describe the AITV-regularized variational models to solve the image ptychography problem. Within this section, we design the stochastic ADMM algorithms to solve these models. Convergence analysis of the stochastic ADMM algorithm follows in Section 4. In Section 5, we illustrate the performance of our proposed stochastic ADMM algorithms and compare them with other competing algorithms. Lastly, in Section 6, we conclude the paper with summary and future works.

2. Preliminaries. In this section, we describe basic notations used throughout the paper.

Let $z \in \mathbb{C}^{n^2}$. The i th entry of z is denoted by $(z)_i$. The vector $\mathbf{1}$ is a vector whose entries are all ones. The vector $\mathbf{0}$ is also defined similarly. The real transpose and conjugate transpose of z are denoted by z^\top and z^* , respectively. The same superscript notations are used for the real transpose and conjugate transpose of matrices. The sign of a complex value $z' \in \mathbb{C}$ is given by

$$\text{sgn}(z') = \begin{cases} \frac{z'}{|z'|} & \text{if } z' \neq 0, \\ c \in \{c' \in \mathbb{C} : |c'| = 1\} & \text{if } z' = 0. \end{cases}$$

The sign of a vector $z \in \mathbb{C}^{n^2}$ is denoted by $\text{sgn}(z)$ and is defined elementwise by $\text{sgn}(z)_i = \text{sgn}(z_i)$, $i = 1, \dots, n^2$. The standard basis vectors of \mathbb{C}^{n^2} are denoted by $\{\mathbf{e}_i\}_{i=1}^{n^2}$, where \mathbf{e}_i is a vector whose i th component is 1 while all other components are zeros. The diagonal matrix of a vector $z \in \mathbb{C}^{n^2}$ is denoted by $D_z = \text{Diag}(z) = z\mathbf{1}^\top \circ I_{n^2 \times n^2}$.

For $p = (p_x, p_y) \in \mathbb{C}^{n^2} \times \mathbb{C}^{n^2}$, its i th entry is $p_i = \begin{bmatrix} (p_x)_i \\ (p_y)_i \end{bmatrix} \in \mathbb{C}^2$. We define the following norms on $\mathbb{C}^{n^2} \times \mathbb{C}^{n^2}$:

$$\begin{aligned} \|p\|_1 &= \sum_{i=1}^{n^2} |(p_x)_i| + |(p_y)_i|, & \|p\|_2 &= \sqrt{\sum_{i=1}^{n^2} |(p_x)_i|^2 + |(p_y)_i|^2}, \\ \|p\|_{2,1} &= \sum_{i=1}^{n^2} \sqrt{|(p_x)_i|^2 + |(p_y)_i|^2} = \sum_{i=1}^{n^2} \|p_i\|_2. \end{aligned}$$

The discrete gradient operator $\nabla : \mathbb{C}^{n^2} \rightarrow \mathbb{C}^{n^2} \times \mathbb{C}^{n^2}$ when specifically applied to the image

z is given by $\nabla z = (\nabla_x z, \nabla_y z)$, where ∇_x and ∇_y are the forward horizontal and vertical difference operators.

We also define the proximal operator of a function $f : \mathbb{C}^{n^2} \rightarrow \mathbb{R} \cup \{+\infty\}$ as

$$\text{prox}_{f(\cdot)}(z') = \arg \min_z f(z) + \frac{1}{2} \|z - z'\|_2^2, \forall z' \in \mathbb{C}^{n^2}.$$

3. Proposed Model. Throughout the paper, we assume that among the mask set $\{S_j\}_{j=1}^N$, there exists j' such that $\|S_{j'} \mathbf{e}_i\|_1 = 1$ for each $i = 1, \dots, n^2$. This assumption ensures that each pixel of an image $z \in \mathbb{C}^{n^2}$ is sampled at least once.

Suppose that the measurements $\{d_j\}_{j=1}^N$ are corrupted by independent and identically distributed (iid) noise, i.e., $d_j \stackrel{\text{iid}}{\sim} \text{Noise}(|\mathcal{F}(\omega \circ S_j z)|^2)$ for $j = 1, \dots, N$. We assume that the noise is either Gaussian or Poisson, both of which are common in phase retrieval. Given an unknown probe ω , the blind variational model [8] is

$$(3.1) \quad \min_{\omega \in \mathbb{C}^{m^2}, z \in \mathbb{C}^{n^2}} \sum_{j=1}^N \mathcal{B}(|\mathcal{F}(\omega \circ S_j z)|^2, d_j),$$

where

$$(3.2) \quad \mathcal{B}(g, f) = \begin{cases} \frac{1}{2} \|\sqrt{g} - \sqrt{f}\|_2^2, & \text{amplitude Gaussian metric (AGM) [51],} \\ \frac{1}{2} \langle g - f \circ \log(g), \mathbf{1} \rangle, & \text{intensity Poisson metric (IPM) [10].} \end{cases}$$

Note that $\sqrt{\cdot}$ is elementwise square root. When the probe ω is known, (3.1) simplifies to the non-blind case as a special case where we only need to find $z \in \mathbb{C}^{n^2}$. Hence, throughout the rest of this section, we will focus on the blind case. To improve image recovery, we propose a class of AITV-regularized variants of (3.1).

3.1. AITV model. For image ptychography, we propose the following AITV-regularized model:

$$(3.3) \quad \min_{\omega \in \mathbb{C}^{m^2}, z \in \mathbb{C}^{n^2}} \sum_{j=1}^N \mathcal{B}(|\mathcal{F}(\omega \circ S_j z)|^2, d_j) + \lambda (\|\nabla z\|_1 - \alpha \|\nabla z\|_{2,1}), \lambda > 0, \alpha \in [0, 1].$$

To develop an ADMM algorithm of (3.3), we introduce auxiliary variables $u = (u_1, \dots, u_N) \in \mathbb{C}^{m^2 \times N}$ and $v = (v_x, v_y) \in \mathbb{C}^{n^2} \times \mathbb{C}^{n^2}$ so that we obtain an equivalent constrained optimization problem

$$(3.4) \quad \min_{u, v, z} \sum_{j=1}^N \mathcal{B}(|u_j|^2, d_j) + \lambda (\|v\|_1 - \alpha \|v\|_{2,1}) \text{ s.t. } u_j = \mathcal{F}(\omega \circ S_j z), j = 1, \dots, N, \text{ and } v = \nabla z.$$

The augmented Lagrangian of (3.4) is

$$(3.5) \quad \mathcal{L}(u, \omega, v, z, \Lambda, y) = \sum_{j=1}^N \left[\mathcal{B}(|u_j|^2, d_j) + \mathbb{R}(\langle \Lambda_j, u_j - \mathcal{F}(\omega \circ S_j z) \rangle) + \frac{\beta_1}{2} \|u_j - \mathcal{F}(\omega \circ S_j z)\|_2^2 \right] \\ + \lambda (\|v\|_1 - \alpha \|v\|_{2,1}) + \mathbb{R}(\langle y, v - \nabla z \rangle) + \frac{\beta_2}{2} \|v - \nabla z\|_2^2,$$

where $\mathbb{R}(\cdot)$ denotes the real component of a complex number; $\langle \cdot, \cdot \rangle$ denotes the complex inner product between two vectors; $\Lambda = (\Lambda_1, \dots, \Lambda_N) \in \mathbb{C}^{m^2 \times N}$ and $y = (y_x, y_y) \in \mathbb{C}^{n^2 \times n^2}$ are Lagrange multipliers; and $\beta_1, \beta_2 > 0$ are penalty parameters. The ADMM algorithm iterates as follows:

$$(3.6a) \quad u^{t+1} \in \arg \min_u \mathcal{L}(u, \omega^t, v^t, z^t, \Lambda^t, y^t),$$

$$(3.6b) \quad \omega^{t+1} \in \arg \min_{\omega} \mathcal{L}(u^{t+1}, \omega, v^t, z^t, \Lambda^t, y^t),$$

$$(3.6c) \quad v^{t+1} \in \arg \min_v \mathcal{L}(u^{t+1}, \omega^{t+1}, v, z^t, \Lambda^t, y^t),$$

$$(3.6d) \quad z^{t+1} \in \arg \min_z \mathcal{L}(u^{t+1}, \omega^{t+1}, v^{t+1}, z, \Lambda^t, y^t),$$

$$(3.6e) \quad \Lambda_j^{t+1} = \Lambda_j^t + \beta_1 \left(u_j^{t+1} - \mathcal{F}(\omega^{t+1} \circ S_j z^{t+1}) \right), \quad j = 1, \dots, N,$$

$$(3.6f) \quad y^{t+1} = y^t + \beta_2 (v^{t+1} - \nabla z^{t+1}).$$

Next we explain how to solve each subproblem.

3.1.1. u -subproblem. In (3.6a), we solve u_j independently of each other. For each $j = 1, \dots, N$, we have

$$(3.7) \quad u_j^{t+1} \in \arg \min_{u_j} \mathcal{B}(|u_j|^2, d_j) + \mathbb{R}(\langle \Lambda_j^t, u_j - \mathcal{F}(P_j^t z^t) \rangle) + \frac{\beta_1}{2} \|u_j - \mathcal{F}(P_j^t z^t)\|_2^2 \\ = \arg \min_{u_j} \frac{1}{\beta_1} \mathcal{B}(|u_j|^2, d_j) + \frac{1}{2} \left\| u_j - \mathcal{F}(P_j^t z^t) + \frac{1}{\beta_1} \Lambda_j^t \right\|_2^2 = \text{prox}_{\frac{1}{\beta_1} \mathcal{B}(|\cdot|^2, d_j)} \left(\mathcal{F}(P_j^t z^t) - \frac{1}{\beta_1} \Lambda_j^t \right),$$

where $P_j^t = \omega^t \circ S_j$. The proximal operator for each fidelity term in (3.2) has a closed-form solution provided in [10, 11], so we have

$$(3.8) \quad u_j^{t+1} = \begin{cases} \frac{\sqrt{d_j + \beta_1} |\mathcal{F}(P_j^t z^t) - \frac{1}{\beta_1} \Lambda_j^t|}{1 + \beta_1} \circ \text{sgn} \left(\mathcal{F}(P_j^t z^t) - \frac{1}{\beta_1} \Lambda_j^t \right), & \text{AGM,} \\ \frac{\beta_1 |\mathcal{F}(P_j^t z^t) - \frac{1}{\beta_1} \Lambda_j^t| + \sqrt{(\beta_1 |\mathcal{F}(P_j^t z^t) - \frac{1}{\beta_1} \Lambda_j^t|)^2 + 4(1 + \beta_1)d_j}}{2(1 + \beta_1)} \circ \text{sgn} \left(\mathcal{F}(P_j^t z^t) - \frac{1}{\beta_1} \Lambda_j^t \right), & \text{IPM.} \end{cases}$$

3.1.2. ω -subproblem. The ω -subproblem (3.6b) can be rewritten as

$$(3.9) \quad \omega^{t+1} \in \arg \min_{\omega} \sum_{j=1}^N \left[\frac{\beta_1}{2} \left\| \mathcal{F}^{-1} \left(u_j^{t+1} + \frac{\Lambda_j^t}{\beta_1} \right) - \omega \circ S_j z^t \right\|_2^2 \right],$$

which shows that updating ω requires access to all N probes. Hence, we develop an alternative update scheme that uses only $b \leq N$ probes. Instead of solving (3.6b) exactly, we linearize it as done in [26, 37] to obtain

$$(3.10) \quad \omega^{t+1} \in \arg \min_{\omega} \langle \nabla_{\omega} \mathcal{L}(u^{t+1}, \omega^t, z^t, \Lambda^t, y^t), \omega - \omega^t \rangle + \frac{1}{2\delta_{\omega}^t} \|\omega - \omega^t\|_2^2$$

for some constant $\delta_{\omega}^t > 0$ at iteration t . Then (3.10) is equivalent to performing gradient descent with step size δ_{ω}^t :

$$(3.11) \quad \omega^{t+1} = \omega^t - \delta_{\omega}^t \nabla_{\omega} \mathcal{L}(u^{t+1}, \omega^t, v^t, z^t, \Lambda^t, y^t).$$

Next we approximate $\nabla_{\omega} \mathcal{L}$ by its stochastic estimator $\tilde{\nabla}_{\omega} \mathcal{L}$. thereby updating ω^{t+1} by SGD with step size $\delta_{\omega}^t > 0$:

$$(3.12) \quad \omega^{t+1} = \omega^t - \delta_{\omega}^t \tilde{\nabla}_{\omega} \mathcal{L}(u^{t+1}, \omega^t, v^t, z^t, \Lambda^t, y^t).$$

We derive some candidates for $\tilde{\nabla}_{\omega} \mathcal{L}$. Let $\mathcal{G}_j^t(\omega) = \frac{\beta_1}{2} \left\| \mathcal{F}^{-1} \left(u_j^{t+1} + \frac{\Lambda_j^t}{\beta_1} \right) - \omega \circ S_j z^t \right\|_2^2$, which means that $\nabla \mathcal{G}_j^t(\omega) = -\beta_1 (S_j z^t)^* \circ \left[\mathcal{F}^{-1} \left(u_j^{t+1} + \frac{\Lambda_j^t}{\beta_1} \right) - \omega \circ S_j z^t \right]$. (3.11) can be rewritten as a gradient descent step with $N\delta_{\omega}^t$:

$$(3.13) \quad \omega^{t+1} = \omega^t - N\delta_{\omega}^t \left(\frac{1}{N} \sum_{j=1}^N \nabla \mathcal{G}_j^t(\omega^t) \right).$$

The SGD estimator [3, 40] of $\frac{1}{N} \sum_{j=1}^N \nabla \mathcal{G}_j^t(\omega^t)$ is $\frac{1}{b} \sum_{j \in n^t} \nabla \mathcal{G}_j^t(\omega^t)$, where $n^t \subset \{1, \dots, N\}$ is a sub-batch of N masks such that $|n^t| = b$. Then the SGD variant (after scaling δ_{ω}^t) of (3.11) is

$$(3.14) \quad \omega^{t+1} = \omega^t - \delta_{\omega}^t \left(\frac{1}{b} \sum_{j \in n^t} \nabla \mathcal{G}_j^t(\omega^t) \right).$$

This implies that one candidate stochastic estimator for $\nabla_{\omega} \mathcal{L}$ is

$$(3.15) \quad \begin{aligned} \tilde{\nabla}_{\omega}^{SGD} \mathcal{L}(u^{t+1}, \omega^t, v^t, z^t, \Lambda^t, y^t) &= \frac{1}{b} \sum_{j \in n^t} \nabla \mathcal{G}_j^t(\omega^t) \\ &= -\frac{\beta_1}{b} \sum_{j \in n^t} (S_j z^t)^* \circ \left[\mathcal{F}^{-1} \left(u_j^{t+1} + \frac{\Lambda_j^t}{\beta_1} \right) - \omega^t \circ S_j z^t \right]. \end{aligned}$$

We can further modify (3.15) by incorporating spatially varying step sizes inspired by the PIE algorithms [32, 33, 42]. Let

$$(3.16) \quad \Phi_j^t = \begin{cases} \frac{\mathbf{1}}{\|S_j z^t\|_\infty^2}, & \text{ePIE [33],} \\ \frac{\|S_j z^t\|_1 \mathbf{1}}{\|S_j z^t\|_\infty (|S_j z^t|^2 + \gamma_\omega \|S_j z^t\|_\infty^2 \mathbf{1})}, & \text{PIE [42],} \\ \frac{\mathbf{1}}{(1 - \gamma_\omega) |S_j z^t|^2 + \gamma_\omega \|S_j z^t\|_\infty^2 \mathbf{1}}, & \text{rPIE [32],} \end{cases}$$

where $\gamma_\omega \in [0, 1]$ for PIE and rPIE and division is elementwise. Incorporating Φ_j^t into (3.15), we have another class of stochastic estimators

$$(3.17) \quad \tilde{\nabla}_\omega^{PIE} \mathcal{L}(u^{t+1}, \omega^t, v^t, z^t, \Lambda^t, y^t) = -\frac{\beta_1}{b} \sum_{j \in n^t} \Phi_j^t \circ (S_j z^t)^* \circ \left[\mathcal{F}^{-1} \left(u_j^{t+1} + \frac{\Lambda_j^t}{\beta_1} \right) - \omega^t \circ S_j z^t \right].$$

3.1.3. v -subproblem. Expanding (3.6c) gives

$$(3.18) \quad \begin{aligned} v^{t+1} &\in \arg \min_v \frac{\lambda}{\beta_2} (\|v\|_1 - \alpha \|v\|_{2,1}) + \frac{1}{2} \left\| v - \nabla z^t + \frac{y^t}{\beta_2} \right\|_2^2 \\ &= \arg \min_v \sum_{i=1}^{n^2} \frac{\lambda}{\beta_2} (\|v_i\|_1 - \alpha \|v_i\|_2) + \frac{1}{2} \left\| v_i - (\nabla z^t)_i + \frac{(y^t)_i}{\beta_2} \right\|_2^2, \end{aligned}$$

which means that the solution v^{t+1} can be solved elementwise. As a result, the subproblem simplifies to

$$(3.19) \quad (v^{t+1})_i = \text{prox}_{\frac{\lambda}{\beta_2} (\|\cdot\|_1 - \alpha \|\cdot\|_2)} \left((\nabla z^t)_i - \frac{(y^t)_i}{\beta_2} \right).$$

A closed-form solution for the proximal operator of $\ell_1 - \alpha \ell_2$ is provided in [27] but only for real-valued vectors. We generalize it to the complex case in Lemma 3.1, whose proof is delayed to Appendix A.

Lemma 3.1. *Given $x' \in \mathbb{C}^n$, $\lambda > 0$. and $\alpha \geq 0$, we have the following cases:*

1. *When $\|x'\|_\infty > \lambda$, we have*

$$x^* = (\|\xi\|_2 + \alpha \lambda) \frac{\xi}{\|\xi\|_2}, \text{ where } \xi = \text{sgn}(x') \circ \max(|x'| - \lambda, 0).$$

2. *When $(1 - \alpha)\lambda < \|x'\|_\infty \leq \lambda$, we have x^* as a 1-sparse vector such that one chooses an index $i \in \arg \max_j (|(x')_j|)$ and have*

$$(x^*)_j = \begin{cases} (|(x')_j| + (\alpha - 1)\lambda) \text{sgn}((x')_j) & \text{if } j = i, \\ 0 & \text{if } j \neq i. \end{cases}$$

3. *When $\|x'\|_\infty \leq (1 - \alpha)\lambda$, we have $x^* = 0$.*

Then x^ is an optimal solution to*

$$(3.20) \quad \text{prox}_{\lambda(\|\cdot\|_1 - \alpha \|\cdot\|_2)}(x') = \arg \min_x \|x\|_1 - \alpha \|x\|_2 + \frac{1}{2\lambda} \|x - x'\|_2^2.$$

3.1.4. z -subproblem. (3.6d) can be rewritten as

$$(3.21) \quad z^{t+1} \in \arg \min_z \sum_{j=1}^N \left[\frac{\beta_1}{2} \left\| u_j^{t+1} - \mathcal{F}(P_j^{t+1} z) + \frac{\Lambda_j^t}{\beta_1} \right\|_2^2 \right] + \frac{\beta_2}{2} \left\| v^{t+1} - \nabla z + \frac{y^t}{\beta_2} \right\|_2^2,$$

which implies that z^{t+1} must satisfy the first-order optimality condition

$$(3.22) \quad \left(\beta_1 \sum_{j=1}^N (P_j^{t+1})^* P_j^{t+1} - \beta_2 \Delta \right) z^{t+1} = \sum_{j=1}^N \beta_1 (P_j^{t+1})^* \mathcal{F}^{-1} \left(u_j^{t+1} + \frac{\Lambda_j^t}{\beta_1} \right) + \beta_2 \nabla^\top \left(v^{t+1} + \frac{y^t}{\beta_2} \right),$$

where the Laplacian $\Delta = -\nabla^\top \nabla$. Since the coefficient matrix of z^{t+1} is invertible, solving (3.22) can be performed exactly, but it could be computationally expensive if the matrix system is extremely large because of the image size of z . Since the coefficient matrix tends to be sparse, conjugate gradient [22] can be used to solve (3.22) like in [10, 11], but it needs access to all N probes and requires at most n^2 iterations to attain an exact solution, assuming exact arithmetic. Moreover, it is sensitive to roundoff error [19].

Alternatively, like in Section 3.1.2 we linearize (3.21) to obtain the gradient descent step with step size $\delta_z^t > 0$:

$$(3.23) \quad z^{t+1} = z^t - \delta_z^t \nabla_z \mathcal{L}(u^{t+1}, \omega^{t+1}, v^{t+1}, z^t, \Lambda^t, y^t).$$

We approximate $\nabla_z \mathcal{L}$ by its stochastic estimator $\tilde{\nabla}_z \mathcal{L}$ that only has access to $b \leq N$ probes. Replacing $\nabla_z \mathcal{L}$ with $\tilde{\nabla}_z \mathcal{L}$ in (3.23) gives

$$(3.24) \quad z^{t+1} = z^t - \delta_z^t \tilde{\nabla}_z \mathcal{L}(u^{t+1}, \omega^{t+1}, v^{t+1}, z^t, \Lambda^t, y^t).$$

To design candidates for $\tilde{\nabla}_z \mathcal{L}$, we will use the following lemma:

Lemma 3.2. *Let $S \in \mathbb{R}^{m^2 \times n^2}$. If $\mathbf{e}_i \in \ker(S)$ for some index i , then for any $x \in \mathbb{C}^{m^2}$, we have $(S^\top x)_i = 0$.*

Proof. We have $(S^\top x)_i = \langle S^\top x, \mathbf{e}_i \rangle = \langle x, S \mathbf{e}_i \rangle = \langle x, 0 \rangle = 0$. ■

For brevity, we denote the vectors

$$(3.25) \quad \begin{aligned} A_j^t &= -\beta_1 \left[(P_j^{t+1})^* \mathcal{F}^{-1} \left(u_j^{t+1} + \frac{\Lambda_j^t}{\beta_1} \right) - (P_j^{t+1})^* P_j^{t+1} z^t \right], \\ B^t &= -\beta_2 \left[\nabla^\top \left(v^{t+1} + \frac{y^t}{\beta_2} \right) + \Delta z^t \right]. \end{aligned}$$

At each element $i = 1, \dots, n^2$, (3.23) becomes

$$(3.26) \quad (z^{t+1})_i = (z^t)_i - \delta_z^t (\nabla_z \mathcal{L}(u^{t+1}, \omega^{t+1}, v^{t+1}, z^t, \Lambda^t, y^t))_i = (z^t)_i - \delta_z^t \left[\sum_{j=1}^N (A_j^t)_i + (B^t)_i \right].$$

By Lemma 3.2, since $(P_j^{t+1})^* = (\omega^{t+1} \circ S_j)^* = S_j^\top D_{(\omega^{t+1})^*}$, we have $(A_j^t)_i = 0$ if $\mathbf{e}_i \in \ker(S_j)$, which means that element i is not scanned by the mask matrix S_j . For each $i = 1, \dots, n^2$, we define $N_i = \{j : \mathbf{e}_i \notin \ker(S_j)\}$ to be the set of indices corresponding to the mask matrices that scan element i . As a result, (3.26) reduces to and can be rewritten as

$$(3.27) \quad (z^{t+1})_i = (z^t)_i - \delta_z^t \left[\sum_{j \in N_i} (A_j^t)_i + (B^t)_i \right] = (z^t)_i - |N_i| \delta_z^t \left[\frac{1}{|N_i|} \sum_{j \in N_i} \left((A_j^t)_i + \frac{1}{|N_i|} (B^t)_i \right) \right].$$

Comparing (3.26) and (3.27), we observe that

$$\frac{1}{|N_i|} \sum_{j \in N_i} \left((A_j^t)_i + \frac{1}{|N_i|} (B^t)_i \right) \propto (\nabla_z \mathcal{L}(u^{t+1}, \omega^{t+1}, v^{t+1}, z^t, \Lambda^t, y^t))_i.$$

Thus, a candidate for the stochastic estimator $\tilde{\nabla}_z \mathcal{L}$ is the SGD estimator $\tilde{\nabla}_z^{SGD} \mathcal{L}$ given by

$$(3.28) \quad \left(\tilde{\nabla}_z^{SGD} \mathcal{L}(u^{t+1}, \omega^{t+1}, v^{t+1}, z^t, \Lambda^t, y^t) \right)_i = \frac{1}{|n_i^t|} \sum_{j \in n_i^t} \left((A_j^t)_i + \frac{1}{|N_i|} (B^t)_i \right),$$

where $n_i^t \subset N_i$ is a mini-batch sampled from N_i at iteration t [3, 40].

We can further modify (3.28) by incorporating spatially varying step sizes inspired by the PIE algorithms [32, 33, 42]. We define

$$(3.29) \quad \Psi_{i,j} = \begin{cases} \frac{1}{\|\omega^{t+1}\|_\infty^2} & \text{ePIE [33],} \\ \frac{\|P_j^{t+1} \mathbf{e}_i\|_1}{\|\omega^{t+1}\|_\infty \left(\|P_j^{t+1} \mathbf{e}_i\|_1^2 + \gamma_z \|\omega^{t+1}\|_\infty^2 \right)} & \text{PIE [42],} \\ \frac{1}{(1 - \gamma_z) \|P_j^{t+1} \mathbf{e}_i\|_1^2 + \gamma_z \|\omega^{t+1}\|_\infty^2} & \text{rPIE [32],} \end{cases}$$

with $\gamma_z \in [0, 1]$ for PIE and rPIE. A class of PIE candidates for the stochastic estimator is

$$(3.30) \quad \left(\tilde{\nabla}_z^{PIE} \mathcal{L}(u^{t+1}, \omega^{t+1}, v^{t+1}, z^t, \Lambda^t, y^t) \right)_i = \frac{1}{|n_i^t|} \sum_{j \in n_i^t} \Psi_{i,j} \left((A_j^t)_i + \frac{1}{|N_i|} (B^t)_i \right).$$

The overall stochastic ADMM algorithm that solves (3.3) is provided by Algorithm 3.1. Notice that the non-blind problem is just a special case with the probe ω fixed.

4. Convergence Analysis. We discuss the convergence of Algorithm 3.1. Although global convergence for ADMM can be established using Kurdyka-Łojasiewicz assumptions [49], the result does not apply for our models because our models contain the gradient operator, which does not satisfy the necessary surjectivity assumption. Hence, we will prove up to subsequential convergence. The convergence analysis is based on the analyses done in [10, 11, 51], where under certain assumptions, they showed that the iterate subsequences of the ADMM

Algorithm 3.1 Stochastic ADMM to solve (3.3)

Input: set of masks $\{S_j\}_{j=1}^N$; model parameters $\lambda > 0$, $\alpha \in [0, 1]$; penalty parameters $\beta_1, \beta_2 > 0$; sequence of step sizes $\{(\delta_\omega^t, \delta_z^t)\}_{t=1}^\infty$; batch size $b \leq N$; PIE factors $\gamma_z, \gamma_\omega \in [0, 1]$.

1: Initialize $\omega^0, z^0, \{u_j^0\}_{j=1}^N = \{\Lambda_j^0\}_{j=1}^N, y^0 = \nabla z^0$.

2: **for** $t = 0$ to $T - 1$ **do**

3: Uniformly sample without replacement the subset $n^t \subset \{1, \dots, N\}$ of batch size b .

4: Compute n_i^t from n^t , i.e., $n_i^t = \sum_{j \in n^t} \|S_j \mathbf{e}_i\|_1$.

5: Update u_j^{t+1} according to (3.8) for each $j \in n^t$.

6: **if** ω is unknown **then**

7: Update $\omega^{t+1} = \omega^t - \delta_\omega^t \tilde{\nabla}_\omega \mathcal{L}(u^{t+1}, \omega^t, v^t, z^t, \Lambda^t, y^t)$. See (3.15) and (3.17) for a candidate $\tilde{\nabla}_\omega \mathcal{L}$.

8: **else**

9: $\omega^{t+1} = \omega^t$.

10: **end if**

11: Compute

$$(v^{t+1})_i = \text{prox}_{\frac{\lambda}{\beta_2}(\|\cdot\|_1 - \alpha\|\cdot\|_2)} \left((\nabla z^t)_i - \frac{(y^t)_i}{\beta_2} \right)$$

for all $i = 1, \dots, n^2$; see Lemma 3.1.

12: Update $(z^{t+1})_i = (z^t)_i - \delta_z^t \left(\tilde{\nabla}_z \mathcal{L}(u^{t+1}, \omega^{t+1}, v^{t+1}, z^t, \Lambda^t, y^t) \right)_i$ for all i such that $n_i^t \neq 0$. See (3.28) and (3.30) for a candidate $\tilde{\nabla}_z \mathcal{L}$.

13: Compute

$$\begin{aligned} \Lambda_j^{t+1} &= \Lambda_j^t + \beta_1 \left(u_j^{t+1} - \mathcal{F}(\omega^{t+1} \circ S_j z^{t+1}) \right), \quad \forall j \in n^t, \\ y^{t+1} &= y^t + \beta_2 (v^{t+1} - \nabla z^{t+1}). \end{aligned}$$

14: **end for**

Output: $\omega^* = \omega^T, z^* = z^T$

algorithms converge to Karush-Kuhn-Tucker (KKT) points. To simplify notation, let $Z = (u, \omega, v, z)$ and $\Omega = (\Lambda, y)$. We also write $\mathcal{L}(\omega)$, for example, to represent the Lagrangian with respect to ω with all other variables fixed at their most recent values. A KKT point (Z^*, Ω^*) of the Lagrangian (3.5) satisfies the KKT conditions given by

$$(4.1a) \quad 0 \in \begin{cases} \partial|u_j^*|(|u_j^*| - \sqrt{d_j}) + \Lambda_j^*, & \text{if AGM,} \\ \partial|u_j^*| \left(|u_j^*| - \frac{\sqrt{d_j}}{|u_j^*|} \right) + \Lambda_j^*, & \text{if IPM,} \end{cases} \quad \text{for } j = 1, \dots, N,$$

$$(4.1b) \quad -\frac{y^*}{\lambda} \in \partial(\|v^*\|_1 - \alpha\|v^*\|_{2,1}),$$

$$(4.1c) \quad u_j^* = \mathcal{F}(\omega^* \circ S_j z^*) \quad \text{for } j = 1, \dots, N,$$

$$(4.1d) \quad v^* = \nabla z^*,$$

$$(4.1e) \quad \nabla_\omega \mathcal{L}(Z^*, \Omega^*) = 0,$$

$$(4.1f) \quad \nabla_z \mathcal{L}(Z^*, \Omega^*) = 0.$$

Because we implement SGD to solve for the probe ω and the image z in the ADMM algorithm, we replace (4.1e) and (4.1f) with the following conditions, respectively:

$$(4.1e') \quad \mathbb{E} \left[\|\nabla_{\omega} \mathcal{L}(Z^*, \Omega^*)\|_2^2 \right] = 0$$

$$(4.1f') \quad \mathbb{E} \left[\|\nabla_z \mathcal{L}(Z^*, \Omega^*)\|_2^2 \right] = 0.$$

We say a point (Z^*, Ω^*) is a stochastic KKT point if it satisfies (4.1a)-(4.1d) and (4.1e')-(4.1f').

Where \mathbb{E}_t denotes the expectation conditioned on the first t iterations of the stochastic ADMM algorithm, we impose the following assumption adapted from [3, Assumption 4.3] relating to the stochastic gradient estimators $\tilde{\nabla}_{\omega} \mathcal{L}$ and $\tilde{\nabla}_z \mathcal{L}$.

Assumption 4.1. *Let $\{(Z^t, \Omega^t)\}_{t=1}^{\infty}$ be a sequence of iterates generated by Algorithm 3.1. Suppose that at each iteration t , the stochastic gradient estimators $\tilde{\nabla}_{\omega} \mathcal{L}(\omega^t) := \tilde{\nabla}_{\omega} \mathcal{L}(u^{t+1}, \omega^t, v^t, z^t, \Lambda^t, y^t)$ and $\tilde{\nabla}_z \mathcal{L}(z^t) := \tilde{\nabla}_z \mathcal{L}(u^{t+1}, \omega^{t+1}, v^{t+1}, z^t, \Lambda^t, y^t)$ satisfy the following:*

(a) *There exist constants $K_U \geq K_L > 0$ such that*

$$(4.3) \quad \mathbb{R} \left(\mathbb{E}_t \left[\langle \nabla_{\omega} \mathcal{L}(\omega^t), \tilde{\nabla}_{\omega} \mathcal{L}(\omega^t) \rangle \right] \right) \geq K_L \mathbb{E}_t \left[\|\nabla_{\omega} \mathcal{L}(\omega^t)\|_2^2 \right]$$

$$(4.4) \quad \left\| \mathbb{E}_t [\tilde{\nabla}_{\omega} \mathcal{L}(\omega^t)] \right\|_2^2 \leq K_U \mathbb{E}_t \left[\|\nabla_{\omega} \mathcal{L}(\omega^t)\|_2^2 \right]$$

$$(4.5) \quad \mathbb{R} \left(\mathbb{E}_t \left[\langle \nabla_z \mathcal{L}(z^t), \tilde{\nabla}_z \mathcal{L}(z^t) \rangle \right] \right) \geq K_L \mathbb{E}_t \left[\|\nabla_z \mathcal{L}(z^t)\|_2^2 \right]$$

$$(4.6) \quad \left\| \mathbb{E}_t [\tilde{\nabla}_z \mathcal{L}(z^t)] \right\|_2^2 \leq K_U \mathbb{E}_t \left[\|\nabla_z \mathcal{L}(z^t)\|_2^2 \right].$$

(b) *There exists constant $M, M_V \geq 0$ such that*

$$(4.7) \quad \mathbb{E}_t \left[\|\tilde{\nabla}_{\omega} \mathcal{L}(\omega^t)\|_2^2 \right] - \left\| \mathbb{E}_t [\tilde{\nabla}_{\omega} \mathcal{L}(\omega^t)] \right\|_2^2 \leq M + M_V \mathbb{E}_t \left[\|\nabla_{\omega} \mathcal{L}(\omega^t)\|_2^2 \right]$$

$$(4.8) \quad \mathbb{E}_t \left[\|\tilde{\nabla}_z \mathcal{L}(z^t)\|_2^2 \right] - \left\| \mathbb{E}_t [\tilde{\nabla}_z \mathcal{L}(z^t)] \right\|_2^2 \leq M + M_V \mathbb{E}_t \left[\|\nabla_z \mathcal{L}(z^t)\|_2^2 \right].$$

To prove the convergence of Algorithm 3.1, we require the following preliminary results. Lemma 4.2 provides useful inequalities while Proposition 4.3 bounds the iterates $\{(Z^t, \Omega^t)\}_{t=1}^{\infty}$ and establishes some bounded property of the gradients $\{(\nabla_{\omega} \mathcal{L}(\omega^t), \nabla_z \mathcal{L}(z^t))\}_{t=1}^{\infty}$.

Lemma 4.2. *Let $\{(Z^t, \Omega^t)\}_{t=1}^{\infty}$ be a sequence of iterates generated by Algorithm 3.1 that satisfies Assumption 4.1. Suppose that $\{(\omega^t, z^t)\}_{t=1}^{\infty}$ is bounded. For each iteration t , we have*

$$(4.9) \quad \mathbb{E}_t[\mathcal{L}(\omega^{t+1})] - \mathbb{E}_t[\mathcal{L}(\omega^t)] \leq - \left(K_L - \frac{\delta_{\omega}^t L_{\omega} (M_V + K_U)}{2} \right) \delta_{\omega}^t \mathbb{E}_t \left[\|\nabla_{\omega} \mathcal{L}(\omega^t)\|_2^2 \right] + \frac{(\delta_{\omega}^t)^2 L_{\omega} M}{2}$$

$$(4.10) \quad \mathbb{E}_t[\mathcal{L}(z^{t+1})] - \mathbb{E}_t[\mathcal{L}(z^t)] \leq - \left(K_L - \frac{\delta_z^t L_z (M_V + K_U)}{2} \right) \delta_z^t \mathbb{E}_t \left[\|\nabla_z \mathcal{L}(z^t)\|_2^2 \right] + \frac{(\delta_z^t)^2 L_z M}{2}$$

for some constants $L_{\omega}, L_z > 0$.

Proposition 4.3. *Let $\{(Z^t, \Omega^t)\}_{t=1}^\infty$ be a sequence of iterates generated by Algorithm 3.1 that satisfies Assumption 4.1. Suppose $\{(\omega^t, z^t)\}_{t=1}^\infty$ is bounded, $\sum_{t=1}^\infty \|\Omega^{t+1} - \Omega^t\|_2^2 < \infty$, and*

$$(4.11) \quad \begin{aligned} \sum_{t=1}^\infty \delta_\omega^t &= \infty, & \sum_{t=1}^\infty (\delta_\omega^t)^2 &< \infty, \\ \sum_{t=1}^\infty \delta_z^t &= \infty, & \sum_{t=1}^\infty (\delta_z^t)^2 &< \infty. \end{aligned}$$

Then $\{(Z^t, \Omega^t)\}_{t=1}^\infty$ is bounded and

$$(4.12) \quad \sum_{t=1}^\infty \mathbb{E} [\delta_\omega^t \|\nabla_\omega \mathcal{L}(\omega^t)\|_2^2 + \delta_z^t \|\nabla_z \mathcal{L}(z^t)\|_2^2] < \infty.$$

The convergence of Algorithm 3.1 is finally established below (see proofs in Appendix B).

Theorem 4.4. *Let $\{(Z^t, \Omega^t)\}_{t=1}^\infty$ be generated by Algorithm 3.1. Under the same assumption as Proposition 4.3, there exists a subsequence of $\{(Z^t, \Omega^t)\}_{t=1}^\infty$ whose accumulation point (Z^*, Ω^*) is a stochastic KKT point almost surely (a.s.) of (3.5).*

We note that the requirement $\sum_{t=1}^\infty \|\Omega^{t+1} - \Omega^t\|_2^2 < \infty$ is rather strong, but similar assumption was made in other nonconvex ADMM algorithms [24, 25, 53] that do not satisfy the necessary assumptions for global convergence [49].

5. Numerical Results. In this section, we evaluate the performance of Algorithm 3.1 on two complex images presented in Figure 2. The probe size used for both images is 256×256 , and the probe is scanned across an image from left to right and top to bottom, giving us $N = 100$ measurements. The measurements $\{d_j\}_{j=1}^N$ are either corrupted by Gaussian noise or Poisson noise. More specifically, when the measurements are corrupted by Gaussian noise, we have

$$(5.1) \quad d_j = (|\mathcal{F}(P_j z)| + \epsilon)^2,$$

where ϵ is an i.i.d. Gaussian random vector. When the measurements are corrupted by Poisson noise, we have

$$(5.2) \quad d_j = \text{Poisson}(|\mathcal{F}(P_j z_\zeta)|),$$

where $z_\zeta = \zeta z$ for some constant $\zeta > 0$. Note that Poisson noise is stronger when ζ is smaller.

For numerical evaluation, we compute the SSIMs [50] of the magnitudes and phases between the reconstructed image z^{**} and the ground-truth image z^g , where $z_i^{**} = \zeta^* z_{i+t^*}^*$ is adjusted for scaling by ζ^* and translation by t^* and $(\zeta^*, t^*) = \arg \min_{\zeta \in \mathbb{C}, t \in \mathbb{Z}} \sum_{i=1}^{n^2} |\zeta z_{i+t}^* - z_i^g|^2$. We compare the proposed stochastic ADMM algorithms with its deterministic, full-batch counterparts (i.e., (3.22) and (3.9) are solved exactly) and its isotropic TV counterparts based on

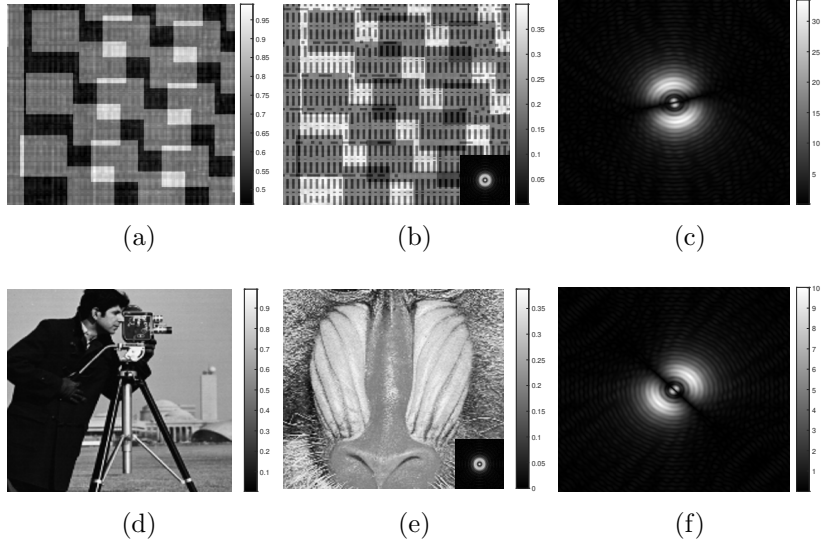


Figure 2: Two complex sample images and their probes examined in the experiments. Left column: sample magnitude; middle column: sample phase with inserted proportionally sized probe magnitude; right column: the magnitude differences between the ground-truth probe and the initial probe ω^0 .

Table 1: Parameter settings for each method. Note that b refers to the batch size.

	Total Epochs	$\beta_1 = \beta_2$	δ_z^t	$\Psi_{i,j}$	δ_ω^t	$\Phi_{i,j}$
AGM	600	0.25	$\begin{cases} 2\sqrt{b} & 1 \leq t \leq 300 \\ \frac{1}{5}\sqrt{b} & 300 < t \leq 450 \\ \frac{1}{50}\sqrt{b} & 450 < t \leq 600 \end{cases}$	rPIE ($\gamma_z = 0.1$)	$\begin{cases} \sqrt{b} \times 10^{-3} & 1 \leq t \leq 300 \\ \sqrt{b} \times 10^{-4} & 300 < t \leq 450 \\ \sqrt{b} \times 10^{-5} & 450 \leq t \leq 600 \end{cases}$	rPIE ($\gamma_\omega = 0.025$)
IPM	300	0.25	$\begin{cases} 15\sqrt{b} & 1 \leq t \leq 150 \\ \frac{3}{5}\sqrt{b} & 150 < t \leq 225 \\ \frac{3}{20}\sqrt{b} & 225 < t \leq 300 \end{cases}$	ePIE	$\begin{cases} 2\sqrt{b} \times 10^{-3} & 1 \leq t \leq 300 \\ 2\sqrt{b} \times 10^{-4} & 300 < t \leq 450 \\ 2\sqrt{b} \times 10^{-5} & 450 \leq t \leq 600 \end{cases}$	ePIE

[10, 11]. The results are also compared with Douglas-Rachford splitting [46], rPIE [33], and PHeBIE [21]. We follow the implementation of Douglas-Rachford from [8].

We initialize $z^0 = \frac{1}{\sqrt{2}}(\mathbf{1} + i\mathbf{1})$ when using AGM for Gaussian-corrupted measurements and $z^0 = \frac{\zeta}{\sqrt{2}}(\mathbf{1} + i\mathbf{1})$ when using IPM for Poisson-corrupted measurements. When performing the blind experiments using Algorithm 3.1, ω^0 is initialized as the perturbation of the ground-truth probe. The magnitude differences between the initial probe and the ground-truth probe are shown in Figure 2. The selected parameters, except for λ , are summarized in Table 1. The initial step sizes for δ_z^t and δ_ω^t are determined empirically, and motivated by (4.11), we decrease them by a factor of 10 at the 1/2 and 3/4 of the total epochs. Decreasing the step size in this way is a popular technique, especially in the deep learning community [18, 20]. Inspired from [18], the step sizes are multiplied by a factor of \sqrt{b} so that they are scaled accordingly to the batch size b . For AITV regularization, we examine $\alpha \in \{0.2, 0.4, 0.6, 0.8\}$

Table 2: SSIM results of the algorithms applied to the Gaussian corrupted measurements with $\text{SNR} = 40$. The stochastic algorithms (e.g., AITV and isoTV, $b \in \{5, 10, 20, 50\}$) are ran three times to obtain the average SSIM values. **Bold** indicates best value; underline indicates second best value.

	Non-blind				Blind			
	Chip		Cameraman/Baboon		Chip		Cameraman/Baboon	
	mag. SSIM	phase SSIM	mag. SSIM	phase SSIM	mag. SSIM	phase SSIM	mag. SSIM	phase SSIM
DR	0.8130	0.8089	0.8701	0.5191	0.8008	0.7642	0.8009	0.3207
rPIE	0.8886	0.9073	0.8930	0.6055	0.9070	0.9120	0.8890	0.6145
PHeBIE	0.8004	0.8019	0.8725	0.5718	0.8612	0.8438	0.8846	0.5756
isoTV ($b = 5$)	0.9501	0.9027	0.9393	0.7578	0.9426	0.8919	0.9324	0.7547
isoTV ($b = 10$)	0.9498	0.9004	0.9387	0.7475	0.9429	0.8891	0.9326	<u>0.7477</u>
isoTV ($b = 20$)	0.9514	0.8981	0.9385	0.7302	0.9447	0.8850	0.9298	0.7289
isoTV ($b = 50$)	0.9355	0.9193	0.9294	0.7050	0.9322	0.9047	0.9153	0.7025
isoTV (full batch)	0.9578	0.9145	<u>0.9769</u>	0.7338	0.9527	0.8698	0.9589	0.5774
AITV ($b = 5$)	0.9585	0.9556	0.9438	<u>0.7720</u>	0.9490	<u>0.9477</u>	0.9373	0.7775
AITV ($b = 10$)	0.9620	<u>0.9579</u>	0.9515	0.7747	<u>0.9534</u>	0.9481	<u>0.9450</u>	0.7772
AITV ($b = 20$)	<u>0.9629</u>	0.9583	0.9538	0.7707	0.9547	0.9470	0.9468	0.7690
AITV ($b = 50$)	0.9585	0.9550	0.9490	0.7358	0.9514	0.9432	0.9391	0.7342
AITV (full batch)	0.9674	0.9513	0.9814	0.7463	0.9676	0.9296	0.9725	0.5956

and determine that $\alpha = 0.8$ yields the best results across all of our numerical examples. The batch sizes we examine are $b \in \{5, 10, 20, 50\}$ for Gaussian noise and $b \in \{5, 10, 20, 25\}$ for Poisson noise. For each parameter setting and image, we run three trials to obtain the mean SSIM values.

The code for the experiments is available at https://github.com/kbui1993/Stochastic-ADMM_Ptycho.

5.1. Gaussian noise. The SNR of the noisy measurements [10] is given by

$$\text{SNR} \left(\left\{ \sqrt{d_j} \right\}_{j=1}^N, \left\{ |\mathcal{F}(P_j z)| \right\}_{j=1}^N \right) = -10 \log_{10} \left(\frac{\sum_{j=1}^N \left\| \sqrt{d_j} - |\mathcal{F}(P_j z)| \right\|_2^2}{\sum_{j=1}^N \left\| \mathcal{F}(P_j z) \right\|_2^2} \right),$$

so determined by the SNR value, the noise level ϵ in (5.1) can be calculated by

$$\epsilon = \sqrt{\frac{10^{-\text{SNR}/10} \sum_{j=1}^N \left\| \mathcal{F}(P_j z) \right\|_2^2}{Nm^2}}.$$

For both the non-blind and blind case, we examine the case when $\text{SNR} = 40$ for the noisy measurements. We set $\lambda = 10.0$. The numerical results are recorded in Table 2. For

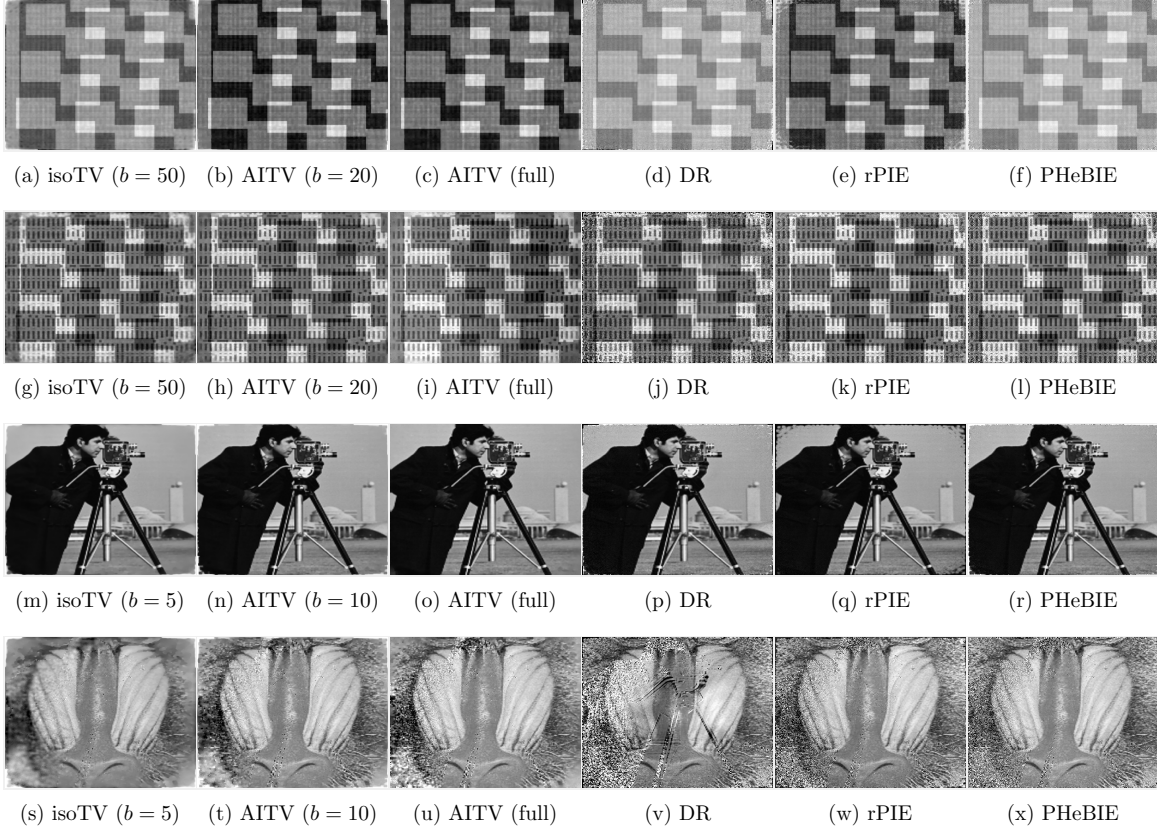


Figure 3: Reconstructions of the non-blind case for the Gaussian noise. Top two rows: reconstructions of Figures 2a-2b; bottom two rows: reconstructions of Figs. 2d-2e.

both the non-blind and blind cases, DR, rPIE, and PHeBIE yield magnitude images with the worst SSIM values, and AITV outperforms its corresponding isotropic TV counterpart by having better SSIM values for both the magnitude and phase images. The stochastic AITV, particularly $b = 10$ or $b = 20$, has slightly lower magnitude SSIM values by at most 0.04 than the best results obtained from the deterministic, full-batch AITV. In fact, stochastic AITV attains the second best magnitude SSIM values in three out of the four cases considered. On the other hand, stochastic AITV with either $b = 10$ or $b = 20$ has the best phase SSIM values, outperforming its deterministic version by up to 0.19. For the blind case of the cameraman/baboon image, the deterministic AITV and isotropic TV have worse phase SSIM values than their stochastic counterparts. In general, the stochastic algorithm does best in recovering phase images with superior SSIM values while recovering the magnitude images with comparable SSIM values as the deterministic algorithm.

The reconstructed images for the non-blind experiments are presented in Figure 3. DR, rPIE, PHeBIE, and the stochastic algorithms have artifacts in all four corners of the magnitude images because the corners are scanned significantly less than in the middle of the image.

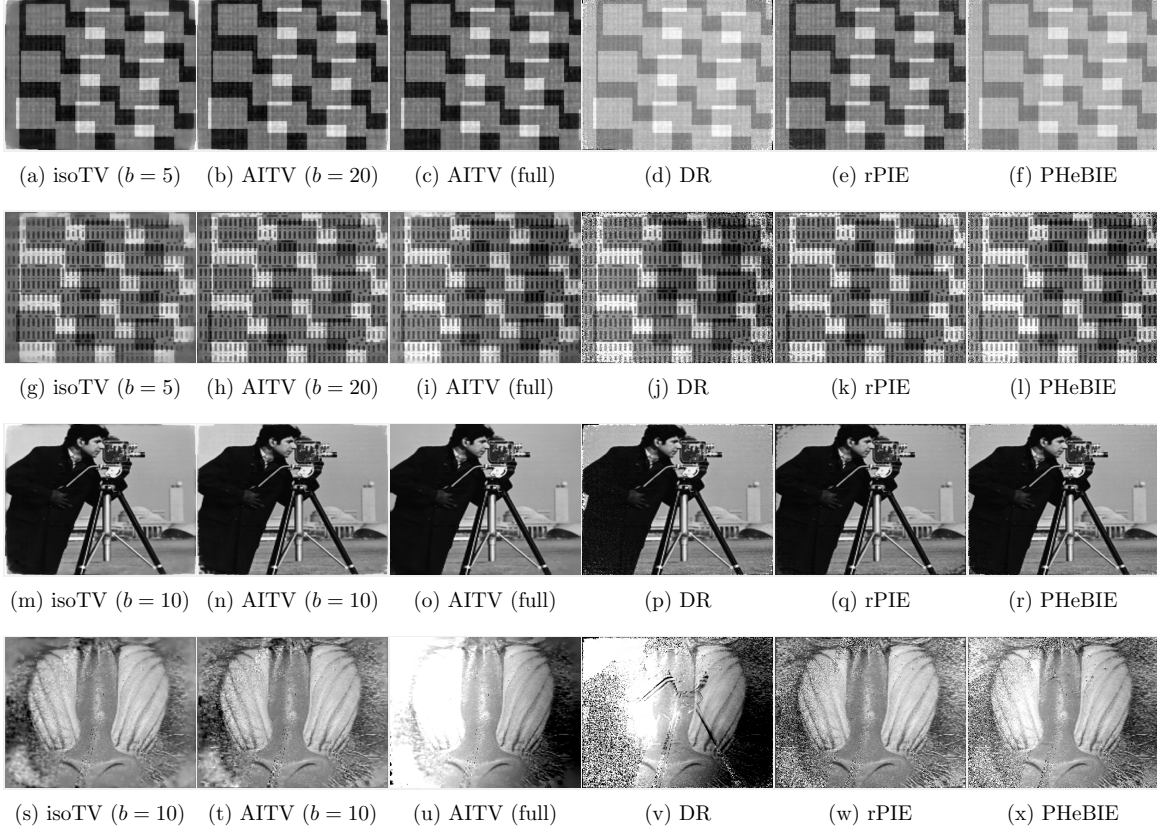


Figure 4: Reconstructions of the blind case for Gaussian noise.

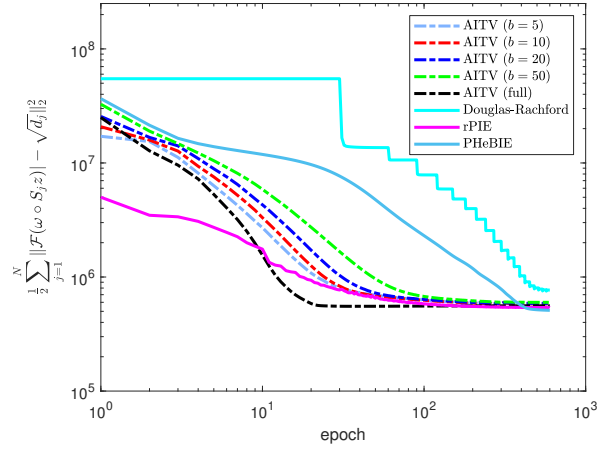


Figure 5: Amplitude Gaussian metric plotted across 600 epochs for the blind algorithms on the complex image given by Figure 2d-2e.

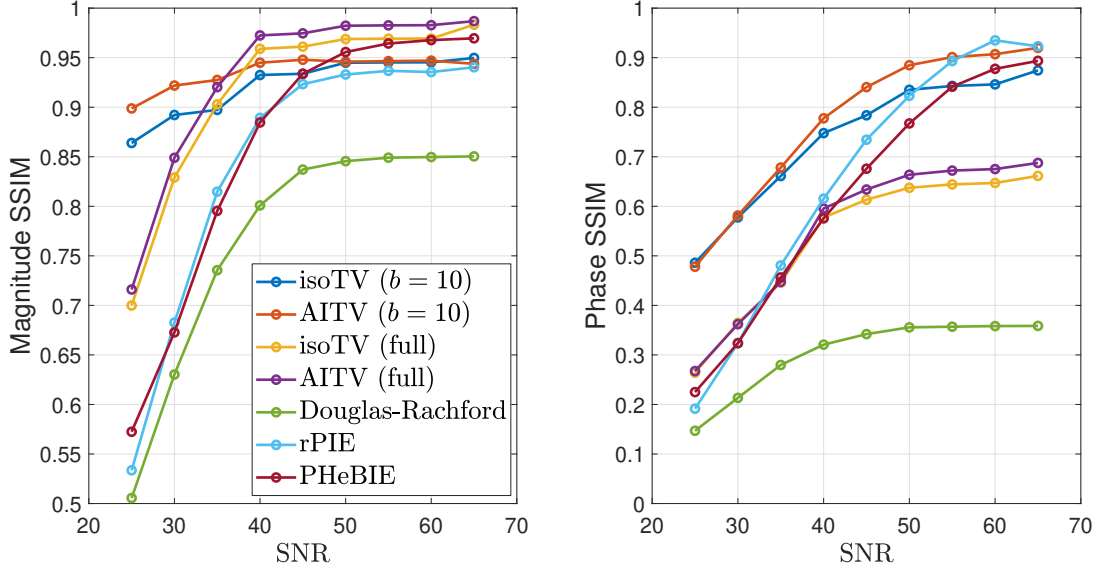


Figure 6: Magnitude and phase SSIMs over different Gaussian noise level for the complex image given by Figure 2d-2e for the blind case.

However, the deterministic AITV has no artifacts because (3.22) is solved exactly for the image solution z . As a result, it has higher magnitude SSIM values than their stochastic counterparts. Nevertheless, the stochastic algorithms yield better phase images with less noise artifacts than any other algorithms. For example, the phase images of Figure 2e reconstructed from stochastic isoTV and AITV have the least amount of cameraman remnants.

Figure 4 shows the results of the blind algorithms. The phase images reconstructed by the deterministic AITV, DR, ePIE and PHeBIE are significantly worse than the stochastic algorithms. For example in Figure 2b, the contrasts of the reconstructed images by the deterministic AITV, DR, and PHeBIE are inconsistent as they become darker from left to right while the contrasts are more consistent with the stochastic algorithms. For Figure 2e, the stochastic algorithms perform the best in recovering the phase image while deterministic AITV is unable to recover the left half of the image and DR, rPIE, and PHeBIE have strong remnants of the cameraman present. Like in the non-blind case, stochastic AITV reconstructs the phase image the best.

In Figure 5, we examine the convergence of the blind algorithms applied to the Camera-man/Baboon image by recording their AGM values for each epoch. We omit the convergence curves for isoTV since their curves are similar to their AITV counterparts. Overall, the curves for our proposed stochastic algorithms are decreasing, validating the numerical convergence of Algorithm 3.1 with AGM fidelity. However, their curves are slightly above the deterministic ADMM algorithm and rPIE. The reason why rPIE outperforms the AITV algorithms is because it seeks to only minimize AGM while the AITV algorithms minimize a larger objective function given by (3.5). Overall, after several hundred epochs, our proposed stochastic algorithms can give comparable AGM values as the deterministic AITV and rPIE algorithms.

Table 3: SSIM results of the algorithms applied to the Poisson corrupted measurements with $\eta = 0.01$. The stochastic algorithms (e.g., AITV and isoTV, $b \in \{5, 10, 20, 25\}$) are ran three times to obtain the average SSIM values. **Bold** indicates best value; underline indicates second best value.

	Non-blind				Blind			
	Chip		Cameraman/Baboon		Chip		Cameraman/Baboon	
	mag. SSIM	phase SSIM	mag. SSIM	phase SSIM	mag. SSIM	phase SSIM	mag. SSIM	phase SSIM
DR	0.8523	0.8455	0.8704	0.5043	0.8431	0.7387	0.7630	0.2529
PHeBIE	0.9404	0.9398	0.9271	0.6791	0.9280	0.9082	0.8678	0.5470
isoTV ($b = 5$)	0.9460	0.9151	0.9301	0.7193	0.9394	0.9001	0.9238	0.7105
isoTV ($b = 10$)	0.9365	0.9212	0.9250	0.7085	0.9342	0.9064	0.9188	0.6979
isoTV ($b = 20$)	0.9335	0.9397	0.9224	0.7008	0.9355	0.9248	0.9153	0.6905
isoTV ($b = 25$)	0.9353	0.9465	0.9220	0.6992	0.9376	0.9315	0.9150	0.6907
isoTV (full batch)	<u>0.9767</u>	0.9590	<u>0.9773</u>	0.7093	<u>0.9655</u>	0.9192	<u>0.9588</u>	0.4920
AITV ($b = 5$)	0.9526	0.9680	0.9319	0.7477	0.9409	<u>0.9530</u>	0.9242	0.7418
AITV ($b = 10$)	0.9590	0.9685	0.9375	<u>0.7366</u>	0.9472	0.9533	0.9321	<u>0.7318</u>
AITV ($b = 20$)	0.9598	<u>0.9682</u>	0.9383	0.7171	0.9494	0.9526	0.9322	0.7114
AITV ($b = 25$)	0.9585	0.9676	0.9373	0.7112	0.9492	0.9525	0.9307	0.7055
AITV (full batch)	0.9803	0.9644	0.9782	0.7084	0.9741	0.9354	0.9671	0.4975

Lastly, we analyze the robustness of the blind algorithms applied to Figures 2d-2e corrupted by different levels of Gaussian noise, from SNR 25 to 65. The fidelity parameter λ varies for different noise level of the image: $\lambda = 100$ for SNR = 25; $\lambda = 50$ for SNR = 30, 35; $\lambda = 10$ for SNR = 40, 45; $\lambda = 5$ for SNR = 50, 55, 60; and $\lambda = 3$ for SNR = 65. The SSIMs for the magnitude and phase images across different SNRs are plotted in Figure 6. For SNR ≥ 40 , the deterministic algorithms have the best magnitude SSIMs than the other algorithms while their stochastic counterparts have slightly lower SSIMs. When SNR < 40 , the stochastic algorithms perform the best. In fact, stochastic AITV has magnitude SSIM at least 0.90 across different noise levels. For the phase image, the stochastic algorithms have the highest SSIMs up to SNR = 55. For SNR ≥ 60 , the rPIE algorithm has the best phase SSIM while stochastic AITV has the second best. Overall, stochastic AITV is the most stable across different levels of Gaussian noise.

5.2. Poisson noise. For both the non-blind and blind case, we examine the measurements corrupted with Poisson noise with $\eta = 0.01$ according to (5.2). We set $\lambda = 0.15$. The numerical results are recorded in Table 3. Note that rPIE results are excluded because the algorithm is tailored towards measurements corrupted with Gaussian noise [32]. Across all cases, deterministic AITV attains the highest magnitude SSIM values and stochastic AITV attains the highest phase SSIM values while DR performs the worst in reconstructing images from Poisson-corrupted measurements. We observe general improvement in SSIM values for both magnitude and phase images by using AITV over isoTV. Although the stochastic algorithms have lower SSIM values than their deterministic counterparts for the magnitude images, the difference is at most 0.047 for AITV and at most 0.056 for isoTV. Moreover, the SSIM values of the magnitude images from the stochastic algorithms are at least 0.91. Similar to the

Gaussian noise case, stochastic AITV reconstructs the phase image well while recovering the magnitude image with satisfactory quality.

We examine the robustness of the blind algorithms on Figures 2d-2e with different level of Poisson noise. The noise levels we examine are $\eta \in \{0.005k\}_{k=1}^9$. We set the fidelity parameter to be $\lambda = 15 \times \eta$. The SSIMs for the magnitude and phase images across different Poisson noise levels are plotted in Figure 7. We observe that the deterministic algorithms yield the best magnitude SSIMs while the stochastic algorithms yield the best phase SSIMs. DR yields the worst results for both magnitude and phase components. Although stochastic AITV yields the third best SSIMs for the magnitude image, its SSIMs are at least 0.90. Moreover, it has the best phase SSIMs, significantly more than its deterministic counterpart by at about 0.20. In summary, stochastic AITV is a robust method across different levels of Poisson noise.

6. Conclusion. In this work, we propose AITV-regularized variational models for image ptychography, where the measurements are corrupted by either Gaussian or Poisson noise. To adapt the algorithm for large number of measurements, we design a stochastic ADMM algorithm that incorporates adaptive step sizes based on the PIE algorithms. Overall, using both AITV regularization and stochastic ADMM, we are able to reconstruct an image of satisfactory quality from heavily corrupted measurements as demonstrated in our numerical experiments. In fact, the phase component of the image is best recovered through our proposed algorithms. Lastly, we prove theoretical convergence for the proposed stochastic ADMM algorithm under certain conditions and demonstrate numerical convergence in our experiments.

Future directions include the design of a globally convergent algorithm for the AITV-regularized ptychography model, and incorporation of variance-reduced stochastic gradient estimators, such as SVRG [23] and SARAH [36], to accelerate convergence and improve reconstruction quality.

Appendix A. Proof of Lemma 3.1.

Proof. If $x' = 0$, then it is trivial, so for the rest of the proof, we assume that $x' \neq 0$.

Suppose x^* is the optimal solution to (3.20). We show that $\text{sgn}(x^*) = \text{sgn}(x')$. If $x^* = 0$, then we can choose $c_i \in \{c' \in \mathbb{C} : |c'| = 1\}$ such that $\text{sgn}(x^*)_i = c_i = \text{sgn}(x')_i$ for each $i = 1, \dots, n^2$, giving the desired result. Suppose that $x^* \neq 0$. Because $\|\cdot\|_1 - \alpha\|\cdot\|_{2,1}$ is rotation invariant, we only need to examine and expand the quadratic term in (3.20). We see that

$$\|x^* - x'\|_2^2 = \sum_{i=1}^{n^2} |(x^*)_i - (x')_i|^2 = \sum_{i=1}^{n^2} (|(x^*)_i|^2 + |(x')_i|^2 - 2|(x^*)_i|| (x')_i| \cos \theta_i),$$

where θ_i is the angle between the components $(x^*)_i$ and $(x')_i$. This term is minimized when $\theta_i = 0$ for all i . This means that $\text{sgn}(x^*)_i = \text{sgn}(x')_i$ for all i , or otherwise x^* would not be an optimal solution to (3.20). Hence, $\text{sgn}(x^*) = \text{sgn}(x')$.

After establishing that $\text{sgn}(x^*) = \text{sgn}(x')$, we simplify (3.20) to an optimization problem with respect to $|x|$ given by

$$|x^*| = \arg \min_{\rho \in \mathbb{R}^n, (\rho)_i \geq 0} \|\rho\|_1 - \alpha\|\rho\|_2 + \frac{1}{2\lambda} \|\rho - |x'|\|_2^2.$$

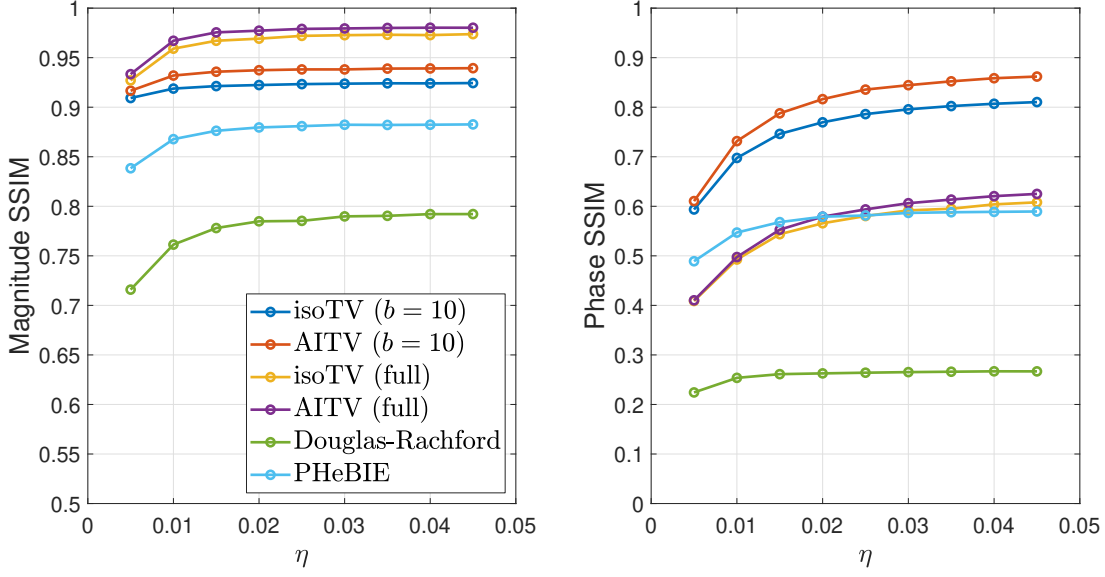


Figure 7: Magnitude and phase SSIMs over different Poisson noise level for the complex image given by Figure 2d-2e for the blind case.

Therefore, by applying [27, Lemma 1] to the optimization problem followed by multiplying the solution $|x^*|$ by $\text{sgn}(x^*)$, we obtain the desired results. ■

Appendix B. Proofs of Section 4. Before proving our main results, we present preliminary tools necessary for the convergence analysis.

Definition B.1 ([41]). Let $h : \mathbb{R}^{n^2} \rightarrow (-\infty, +\infty]$ be a proper and lower semicontinuous function and $\text{dom } h := \{x \in \mathbb{R}^{n^2} : h(x) < \infty\}$.

(a) The Fréchet subdifferential of h at the point $x \in \text{dom } h$ is the set

$$\hat{\partial}h(x) = \left\{ v \in \mathbb{R}^{n^2} : \liminf_{y \neq x, y \rightarrow x} \frac{h(y) - h(x) - \langle v, y - x \rangle}{\|y - x\|} \geq 0 \right\}.$$

(b) The limiting subdifferential of h at the point $x \in \text{dom } h$ is the set

$$\partial h(x) = \left\{ v \in \mathbb{R}^{n^2} : \exists \{(x^t, y^t)\}_{t=1}^\infty \text{ s.t. } x^t \rightarrow x, h(x^t) \rightarrow h(x), \hat{\partial}h(x^t) \ni y^t \rightarrow v \right\}.$$

We note that the limiting subdifferential is closed [41]:

$$(x^t, y^t) \rightarrow (x, y), h(x^t) \rightarrow h(x), y^t \in \partial h(x^t) \implies y \in \partial h(x).$$

After establishing the definitions of subdifferentials in the real case, we extend them to the complex case. If $z = z_1 + z_2 \mathbf{i}$, where $z_1, z_2 \in \mathbb{R}^{n^2}$, then the limiting subdifferential of a proper and lower semicontinuous function $f : \mathbb{C}^{n^2} \rightarrow (-\infty, +\infty]$ is defined by

$$(B.1) \quad \partial f(z) := \partial_{z_1} f(z) + \partial_{z_2} f(z) \mathbf{i}.$$

If the function f is continuously differentiable at the point z , then with slight abuse of notation, we denote its gradient by $\nabla f(z)$, and $\partial f(z) = \{\nabla f(z)\}$ [41].

B.1. Proof of Lemma 4.2.

Proof. If $\{(\omega^t, z^t)\}_{t=1}^\infty$ is bounded, then there exists a constant C such that $\|\omega^t\|_\infty, \|z^t\|_\infty \leq C$ for all $t \in \mathbb{N}$. We establish that $\mathcal{L}(\omega)$ has a Lipschitz continuous gradient with respect to ω . For any $\omega_1, \omega_2 \in \mathbb{C}^{m^2}$ at iteration t , we have

$$\begin{aligned} \|\nabla_\omega \mathcal{L}(\omega_2) - \nabla_\omega \mathcal{L}(\omega_1)\|_2 &\leq \left\| \sum_{j=1}^N \beta_1 (S_j z^t)^* \circ (\omega_2 - \omega_1) \circ (S_j z^t) \right\|_2 \\ &\leq \left[\sum_{j=1}^N \beta_1 \|(S_j z^t)^* \circ (S_j z^t)\|_\infty \right] \|\omega_2 - \omega_1\|_2 \leq \beta_1 N C^2 \|\omega_2 - \omega_1\|_2. \end{aligned}$$

Hence, we observe that $\mathcal{L}(\omega)$ has a Lipschitz continuous gradient with Lipschitz constant $L_\omega := \beta_1 N C^2$. By the descent property [8, Definition 1], at iteration t we have

$$\begin{aligned} \mathcal{L}(\omega^{t+1}) - \mathcal{L}(\omega^t) &\leq \mathbb{R}(\langle \nabla_\omega \mathcal{L}(\omega^t), \omega^{t+1} - \omega^t \rangle) + \frac{L_\omega}{2} \|\omega^{t+1} - \omega^t\|_2^2 \\ &= -\delta_\omega^t \mathbb{R}(\langle \nabla_\omega \mathcal{L}(\omega^t), \tilde{\nabla}_\omega \mathcal{L}(\omega^t) \rangle) + \frac{L_\omega (\delta_\omega^t)^2}{2} \|\tilde{\nabla}_\omega \mathcal{L}(\omega^t)\|_2^2, \end{aligned}$$

where the last equality is due to (3.12). Taking the expectation with respect to the first t iterations, we obtain

$$\begin{aligned} \mathbb{E}_t[\mathcal{L}(\omega^{t+1})] - \mathbb{E}_t[\mathcal{L}(\omega^t)] &= -\delta_\omega^t \mathbb{R} \left(\mathbb{E}_t \left[\langle \nabla_\omega \mathcal{L}(\omega^t), \tilde{\nabla}_\omega \mathcal{L}(\omega^t) \rangle \right] \right) + \frac{L_\omega (\delta_\omega^t)^2}{2} \mathbb{E}_t \left[\|\tilde{\nabla}_\omega \mathcal{L}(\omega^t)\|_2^2 \right] \\ &\leq - \left(K_L - \frac{\delta_\omega^t L_\omega (M_V + K_U)}{2} \right) \delta_\omega^t \mathbb{E}_t \left[\|\nabla_\omega \mathcal{L}(\omega^t)\|_2^2 \right] + \frac{(\delta_\omega^t)^2 L_\omega M}{2}, \end{aligned}$$

where the last inequality is due to combining (4.3), (4.4). and (4.7). Similarly, we can estimate (4.10) because we can compute that $\mathcal{L}(z)$ has a Lipschitz continuous gradient with Lipschitz constant $L_z := \beta_1 N C^2 + \beta_2 \|\Delta\|$ and follow the same steps as above. ■

B.2. Proof of Proposition 4.3.

Proof. Because $\sum_{t=1}^\infty \|\Omega^{t+1} - \Omega^t\|_2^2 < \infty$, we have $\lim_{t \rightarrow \infty} \Lambda_j^{t+1} - \Lambda_j^t = 0$ for each $j = 1, \dots, N$ and $\lim_{t \rightarrow \infty} y^{t+1} - y^t = 0$, which implies from (3.6e)-(3.6f) that

$$(B.2) \quad \lim_{t \rightarrow \infty} u_j^t - \mathcal{F}(\omega^t \circ S_j z^t) = 0 \quad \forall j = 1, \dots, N,$$

$$(B.3) \quad \lim_{t \rightarrow \infty} v^t - \nabla z^t = 0.$$

It follows that $\{(u^t, v^t)\}_{t=1}^\infty$ is bounded since $\{(\omega^t, z^t)\}_{t=1}^\infty$ is bounded. By (3.8), when $\mathcal{B}(\cdot, \cdot)$ is AGM, we have

$$\|u_j^{t+1}\|_2 = \left\| \frac{\sqrt{d_j} + \beta_1 \left| \mathcal{F}(\omega^t \circ S_j z^t) - \frac{1}{\beta_1} \Lambda_j^t \right|}{1 + \beta_1} \right\|_2 \geq \frac{\beta_1}{1 + \beta_1} \left(\frac{1}{\beta_1} \|\Lambda_j^t\|_2 - \|\mathcal{F}(\omega^t \circ S_j z^t)\|_2 \right),$$

or equivalently,

$$(B.4) \quad (1 + \beta_1)\|u_j^{t+1}\|_2 + \beta_1\|\mathcal{F}(\omega^t \circ S_j z^t)\|_2 \geq \|\Lambda_j^t\|_2.$$

Similarly, when $\mathcal{B}(\cdot, \cdot)$ is IPM, we have the same inequality as (B.4). As a result, $\{\Lambda_j^t\}_{t=1}^\infty$ is bounded. Finally, we show that $\{y^t\}_{t=1}^\infty$ is bounded. By Lemma 3.1, we have two cases. When

$$\left\|(\nabla z^t)_i - \frac{(y^t)_i}{\beta_2}\right\|_\infty \leq \frac{\lambda}{\beta_2},$$

we have

$$\frac{\lambda}{\beta_2} \geq \left\|(\nabla z^t)_i - \frac{(y^t)_i}{\beta_2}\right\|_\infty \geq \frac{1}{\beta_2} \|(y^t)_i\|_\infty - \|(\nabla z^t)_i\|_\infty,$$

or $\lambda + \beta_2\|(\nabla z^t)_i\|_\infty \geq \|(y^t)_i\|_\infty$. Otherwise, we have

$$\begin{aligned} \|(v^{t+1})_i\|_\infty &\geq \left\|(\nabla z^t)_i - \frac{(y^t)_i}{\beta_2} - \frac{\lambda}{\beta_2}\right\|_\infty \geq \left\|(\nabla z^t)_i - \frac{(y^t)_i}{\beta_2}\right\|_\infty - \frac{\lambda}{\beta_2} \\ &\geq \frac{1}{\beta_2} \|(y^t)_i\|_\infty - \|(\nabla z^t)_i\|_\infty - \frac{\lambda}{\beta_2}, \end{aligned}$$

or $\beta_2(\|(v^{t+1})_i\|_\infty + \|(\nabla z^t)_i\|_\infty) + \lambda \geq \|(y^t)_i\|_\infty$. Altogether, $\{y^t\}_{t=1}^\infty$ is bounded since $\{(v^t, z^t)\}_{t=1}^\infty$ is bounded. Therefore, we establish that $\{(Z^t, \Omega^t)\}_{t=1}^\infty$ is bounded.

We see that

$$\begin{aligned} \mathcal{L}(Z, \Omega) &= \sum_{j=1}^N \left[\mathcal{B}(|u_j|^2, d_j) + \frac{\beta_1}{2} \left\| u_j - \mathcal{F}(\omega \circ S_j z) + \frac{\Lambda_j}{\beta_1} \right\|_2^2 - \frac{1}{2\beta_1} \|\Lambda_j\|_2^2 \right] \\ &\quad + \lambda(\|v\|_1 - \alpha\|v\|_{2,1}) + \frac{\beta_2}{2} \left\| v - \nabla z + \frac{y}{\beta_2} \right\|_2^2 - \frac{1}{2\beta_2} \|y\|_2^2 \\ &\geq \sum_{j=1}^N \left[\mathcal{B}(|u_j|^2, d_j) - \frac{1}{2\beta_1} \|\Lambda_j\|_2^2 \right] - \frac{1}{2\beta_2} \|y\|_2^2. \end{aligned}$$

Because $\mathcal{B}(\cdot, \cdot)$ is bounded below according to (3.2) and $\{\Omega^t\}_{t=1}^\infty$ is bounded, $\{\mathcal{L}(Z^t, \Omega^t)\}_{t=1}^\infty$ is bounded below by some constant \mathcal{L}_{\inf} . By (3.6a) and (3.6c), we have $\mathcal{L}(u^{t+1}) \leq \mathcal{L}(u^t)$ and $\mathcal{L}(v^{t+1}) \leq \mathcal{L}(v^t)$, respectively, so taking expectation with respect to the first t iterations, we obtain

$$(B.5) \quad \mathbb{E}_t[\mathcal{L}(\omega^t)] = \mathbb{E}_t[\mathcal{L}(u^{t+1})] \leq \mathbb{E}_t[\mathcal{L}(u^t)],$$

$$(B.6) \quad \mathbb{E}_t[\mathcal{L}(z^t)] = \mathbb{E}_t[\mathcal{L}(v^{t+1})] \leq \mathbb{E}_t[\mathcal{L}(v^t)] = \mathbb{E}_t[\mathcal{L}(\omega^{t+1})].$$

In addition, we have

$$\mathcal{L}(\Lambda^{t+1}) - \mathcal{L}(\Lambda^t) = \sum_{j=1}^N \mathbb{R}(\langle \Lambda_j^{t+1} - \Lambda_j^t, u_j^{t+1} - \mathcal{F}(\omega^{t+1} \circ S_j z^{t+1}) \rangle)$$

$$= \frac{1}{\beta_1} \sum_{j=1}^N \left\| \Lambda_j^{t+1} - \Lambda_j^t \right\|_2^2 = \frac{1}{\beta_1} \left\| \Lambda^{t+1} - \Lambda^t \right\|_2^2,$$

where the second to last equality is due to (3.6e). Taking expectation with respect to the first t iterations gives

$$(B.7) \quad \mathbb{E}_t[\mathcal{L}(\Lambda^{t+1})] - \mathbb{E}_t[\mathcal{L}(\Lambda^t)] = \frac{1}{\beta_1} \mathbb{E}_t \left[\left\| \Lambda^{t+1} - \Lambda^t \right\|_2^2 \right].$$

Similarly, we obtain

$$(B.8) \quad \mathbb{E}_t[\mathcal{L}(y^{t+1})] - \mathbb{E}_t[\mathcal{L}(y^t)] = \frac{1}{\beta_2} \mathbb{E}_t [\|y^{t+1} - y^t\|_2^2].$$

Summing up (4.9)-(4.10), (B.5)-(B.8) and taking total expectation, we have

$$(B.9) \quad \begin{aligned} \mathbb{E}[\mathcal{L}(Z^{t+1}, \Omega^{t+1})] - \mathbb{E}[\mathcal{L}(Z^t, \Omega^t)] &\leq \frac{1}{\beta_1} \mathbb{E}_t \left[\left\| \Lambda^{t+1} - \Lambda^t \right\|_2^2 \right] + \frac{1}{\beta_2} \mathbb{E} [\|y^{t+1} - y^t\|_2^2] \\ &\quad - \left(K_L - \frac{\delta_\omega^t L_\omega (M_V + K_U)}{2} \right) \delta_\omega^t \mathbb{E} \left[\left\| \nabla_\omega \mathcal{L}(\omega^t) \right\|_2^2 \right] + \frac{(\delta_\omega^t)^2 L_\omega M}{2} \\ &\quad - \left(K_L - \frac{\delta_z^t L_z (M_V + K_U)}{2} \right) \delta_z^t \mathbb{E} \left[\left\| \nabla_z \mathcal{L}(z^t) \right\|_2^2 \right] + \frac{(\delta_z^t)^2 L_z M}{2}. \end{aligned}$$

By (4.11), $\lim_{t \rightarrow \infty} \delta_\omega^t = 0$ and $\lim_{t \rightarrow \infty} \delta_z^t = 0$, which means that we can assume without generality that $\delta_\omega^t L_\omega, \delta_z^t L_z < \frac{K_L}{M_V + K_U}$ for all $t \in \mathbb{N}$. Hence, summing up $t = 1, \dots, T$, we obtain

$$\begin{aligned} \mathcal{L}_{\inf} - \mathbb{E}[\mathcal{L}(Z^0, \Omega^0)] &\leq \mathbb{E}[\mathcal{L}(Z^{T+1}, \Omega^{T+1})] - \mathbb{E}[\mathcal{L}(Z^0, \Omega^0)] \\ &\leq \sum_{t=1}^T \left(C \left\| \Omega^{t+1} - \Omega^t \right\|_2^2 - \frac{K_L \delta_\omega^t}{2} \mathbb{E} \left[\left\| \nabla_\omega \mathcal{L}(\omega^t) \right\|_2^2 \right] - \frac{K_L \delta_z^t}{2} \mathbb{E} \left[\left\| \nabla_z \mathcal{L}(z^t) \right\|_2^2 \right] \right. \\ &\quad \left. + \frac{(\delta_\omega^t)^2 L_\omega M}{2} + \frac{(\delta_z^t)^2 L_z M}{2} \right), \end{aligned}$$

where $C = \max\{\frac{1}{\beta_1}, \frac{1}{\beta_2}\}$. Rearranging the inequality and letting $T \rightarrow \infty$ give us

$$\begin{aligned} 0 &\leq \frac{K_L}{2} \sum_{t=1}^{\infty} \left(\delta_\omega^t \mathbb{E} \left[\left\| \nabla_\omega \mathcal{L}(\omega^t) \right\|_2^2 \right] + \delta_z^t \mathbb{E} \left[\left\| \nabla_z \mathcal{L}(z^t) \right\|_2^2 \right] \right) \leq \\ &\quad \mathbb{E}[\mathcal{L}(Z^0, \Omega^0)] - \mathcal{L}_{\inf} + \sum_{t=1}^{\infty} \left(C \left\| \Omega^{t+1} - \Omega^t \right\|_2^2 + \frac{(\delta_\omega^t)^2 L_\omega M}{2} + \frac{(\delta_z^t)^2 L_z M}{2} \right). \end{aligned}$$

By the assumption, the right-hand side is bounded, so therefore it implies (4.12). ■

B.3. Proof of Theorem 4.4.

Proof. If $\{(w^t, z^t)\}_{t=1}^\infty$ is bounded, then $\|w^t\|_2, \|z^t\|_2 \leq C$ for all $t \in \mathbb{N}$ for some constant $C > 0$. At a given iteration t , we have $\nabla_\omega \mathcal{L}(\omega^{t+1}) = 0$ by the first-order optimality condition of (3.6b) and $\nabla_\omega \mathcal{L}(\omega)$ to be Lipschitz. It follows that

$$\|\nabla_\omega \mathcal{L}(\omega^t)\|_2 = \|\nabla_\omega \mathcal{L}(\omega^{t+1}) - \nabla_\omega \mathcal{L}(\omega^t)\|_2 \leq L_\omega \|\omega^{t+1} - \omega^t\|_2 \leq 2CL_\omega.$$

Similarly, we have $\|\nabla_z \mathcal{L}(z^t)\|_2 \leq 2CL_z$. As a result, by squaring the inequalities and taking their expectation, $\left\{ \left(\mathbb{E} \left[\|\nabla_\omega \mathcal{L}(\omega^t)\|_2^2 \right], \mathbb{E} \left[\|\nabla_z \mathcal{L}(z^t)\|_2^2 \right] \right) \right\}_{t=1}^\infty$ is bounded. The step size condition (4.11) implies that $\lim_{t \rightarrow \infty} \delta_\omega^t = 0$ and $\lim_{t \rightarrow \infty} \delta_z^t = 0$. Since the SGD steps for ω and z are

$$\omega^{t+1} = \omega^t - \delta_\omega^t \tilde{\nabla} \mathcal{L}(\omega^t), \quad z^{t+1} = z^t - \delta_z^t \tilde{\nabla} \mathcal{L}(z^t),$$

it follows that by taking expectation with respect to the first t iterations and using Assumption 4.1,

$$\begin{aligned} \mathbb{E}_t[\|\omega^{t+1} - \omega^t\|_2^2] &= (\delta_\omega^t)^2 \mathbb{E}_t[\|\tilde{\nabla}_\omega \mathcal{L}(\omega^t)\|_2^2] \leq (\delta_\omega^t)^2 \left(M + (M_V + K_U) \mathbb{E}_t[\|\nabla_\omega \mathcal{L}(\omega^t)\|_2^2] \right), \\ \mathbb{E}_t[\|z^{t+1} - z^t\|_2^2] &= (\delta_z^t)^2 \mathbb{E}_t[\|\tilde{\nabla}_z \mathcal{L}(z^t)\|_2^2] \leq (\delta_z^t)^2 \left(M + (M_V + K_U) \mathbb{E}_t[\|\nabla_z \mathcal{L}(z^t)\|_2^2] \right). \end{aligned}$$

Because $\left\{ \left(\mathbb{E}[\|\nabla_\omega \mathcal{L}(\omega^t)\|_2^2], \mathbb{E}[\|\nabla_z \mathcal{L}(z^t)\|_2^2] \right) \right\}_{t=1}^\infty$ is bounded, we apply total expectation and take the limit to obtain

$$(B.10) \quad \lim_{t \rightarrow \infty} \mathbb{E}[\|\omega^{t+1} - \omega^t\|_2^2] \leq \lim_{t \rightarrow \infty} (\delta_\omega^t)^2 \left(M + (M_V + K_U) \mathbb{E}[\|\nabla_\omega \mathcal{L}(\omega^t)\|_2^2] \right) = 0,$$

$$(B.11) \quad \lim_{t \rightarrow \infty} \mathbb{E}[\|z^{t+1} - z^t\|_2^2] \leq \lim_{t \rightarrow \infty} (\delta_z^t)^2 \left(M + (M_V + K_U) \mathbb{E}[\|\nabla_z \mathcal{L}(z^t)\|_2^2] \right) = 0.$$

Earlier, in the proof of Proposition 4.3, we obtain

$$(B.12) \quad \lim_{t \rightarrow \infty} u_j^t - \mathcal{F}(\omega^t \circ S_j z^t) = 0, \quad \forall j = 1, \dots, N,$$

$$(B.13) \quad \lim_{t \rightarrow \infty} v^t - \nabla z^t = 0.$$

By Proposition 4.3, we have $\{(Z^t, \Omega^t)\}_{t=1}^\infty$ to be bounded and (4.12) to be true.

Because $\{Z^t\}_{t=1}^\infty$ is bounded, there exists a convergent subsequence $\{(Z^{t_k}, \Omega^{t_k})\}_{k=1}^\infty$ and a point (Z^*, Ω^*) such that $\lim_{k \rightarrow \infty} (Z^{t_k}, \Omega^{t_k}) = (Z^*, \Omega^*)$. In addition, (4.12) and (B.10)-(B.13) hold for the subsequence and its further subsequences. (B.10)-(B.11) imply that there is a further subsequence $\{(Z^{t_{k_\ell}}, \Omega^{t_{k_\ell}})\}_{\ell=1}^\infty$ such that

$$(B.14) \quad \lim_{\ell \rightarrow \infty} \omega^{t_{k_\ell}+1} - \omega^{t_{k_\ell}} = 0 \text{ a.s.},$$

$$(B.15) \quad \lim_{\ell \rightarrow \infty} z^{t_{k_\ell}+1} - z^{t_{k_\ell}} = 0 \text{ a.s.}$$

From (4.12), we obtain $\lim_{\ell \rightarrow \infty} \mathbb{E} \left[\delta_{\omega}^{t_{k_\ell}} \|\nabla_{\omega} \mathcal{L}(\omega^{t_{k_\ell}})\|_2^2 + \delta_z^{t_{k_\ell}} \|\nabla_z \mathcal{L}(z^{t_{k_\ell}})\|_2^2 \right] = 0$, so we obtain

$$(B.16) \quad \liminf_{\ell \rightarrow \infty} \mathbb{E}[\|\nabla_{\omega} \mathcal{L}(\omega^{t_{k_\ell}})\|_2^2] = 0$$

$$(B.17) \quad \liminf_{\ell \rightarrow \infty} \mathbb{E}[\|\nabla_z \mathcal{L}(z^{t_{k_\ell}})\|_2^2] = 0.$$

Now we show that (Z^*, Ω^*) is a stochastic KKT point a.s. From (B.12)-(B.13), we have

$$(B.18) \quad u_j^* = \lim_{\ell \rightarrow \infty} u_j^{t_{k_\ell}} = \lim_{\ell \rightarrow \infty} \mathcal{F}(\omega^{t_{k_\ell}} \circ S_j z^{t_{k_\ell}}) = \mathcal{F}(\omega^* \circ S_j z^*),$$

$$(B.19) \quad v^* = \lim_{\ell \rightarrow \infty} v^{t_{k_\ell}} = \lim_{\ell \rightarrow \infty} \nabla_z \mathcal{L}(z^{t_{k_\ell}}) = \nabla_z \mathcal{L}(z^*).$$

By (B.12) and (B.14)-(B.15), we have

$$\begin{aligned} \lim_{\ell \rightarrow \infty} u^{t_{k_\ell}+1} &= \lim_{\ell \rightarrow \infty} \mathcal{F}(\omega^{t_{k_\ell}+1} \circ S_j z^{t_{k_\ell}+1}) = \mathcal{F}\left(\lim_{\ell \rightarrow \infty} \omega^{t_{k_\ell}+1} \circ S_j \left(\lim_{\ell \rightarrow \infty} z^{t_{k_\ell}+1}\right)\right) \\ &= \mathcal{F}\left(\lim_{\ell \rightarrow \infty} \omega^{t_{k_\ell}} \circ S_j \left(\lim_{\ell \rightarrow \infty} z^{t_{k_\ell}}\right)\right) = \lim_{\ell \rightarrow \infty} \mathcal{F}(\omega^{t_{k_\ell}} \circ S_j z^{t_{k_\ell}}) = \lim_{\ell \rightarrow \infty} u^{t_{k_\ell}} \text{ a.s.} \end{aligned}$$

As a result, we have

$$(B.20) \quad \lim_{\ell \rightarrow \infty} u^{t_{k_\ell}+1} - u^{t_{k_\ell}} = 0 \text{ a.s.}$$

Similarly, by (B.13) and (B.15), we have

$$(B.21) \quad \lim_{\ell \rightarrow \infty} v^{t_{k_\ell}+1} - v^{t_{k_\ell}} = 0 \text{ a.s.}$$

For the sake of brevity, we will omit “a.s.” henceforth.

Next we prove (4.1a). Suppose that $\mathcal{B}(\cdot, \cdot)$ is AGM. At iteration t_{k_ℓ} , the first-order optimality condition of (3.6a) is

$$(B.22) \quad 0 \in \partial \left| u_j^{t_{k_\ell}+1} \right| \left(\left| u_j^{t_{k_\ell}+1} \right| - \sqrt{d_j} \right) + \Lambda_j^{t_{k_\ell}} + \beta_1 \left(u_j^{t_{k_\ell}+1} - \mathcal{F}(\omega^{t_{k_\ell}} \circ S_j z^{t_{k_\ell}}) \right),$$

where

$$\left(\partial \left| u_j^{t_{k_\ell}+1} \right| \right)_i = \begin{cases} \frac{(u_j^{t_{k_\ell}+1})_i}{|(u_j^{t_{k_\ell}+1})_i|}, & \text{if } (u_j^{t_{k_\ell}+1})_i \neq 0 \\ \{u \in \mathbb{C} : |u| \leq 1\} & \text{if } (u_j^{t_{k_\ell}+1})_i = 0. \end{cases}$$

If $(u_j^*)_i \neq 0$ for some $i \in \{1, \dots, n^2\}$, then there exists a neighborhood $B_r((u_j^*)_i) = \{u \in \mathbb{C} : |u - (u_j^*)_i| \leq r\}$ such that all points in $B_r((u_j^*)_i)$ are nonzero. By (B.20) and the fact that $\lim_{\ell \rightarrow \infty} u^{t_{k_\ell}} = u^*$, we have $(u_j^{t_{k_\ell}+1})_i \neq 0$ for all t_{k_ℓ} sufficiently large. As a result, (B.22) becomes

$$(B.23) \quad 0 = \frac{(u_j^{t_{k_\ell}+1})_i}{|(u_j^{t_{k_\ell}+1})_i|} \left(|(u_j^{t_{k_\ell}+1})_i| - (\sqrt{d_j})_i \right) + (\Lambda_j^{t_{k_\ell}})_i + \beta_1 \left((u_j^{t_{k_\ell}+1})_i - (\mathcal{F}(\omega^{t_{k_\ell}} \circ S_j z^{t_{k_\ell}}))_i \right),$$

By (B.12) and (B.20), we take the limit to obtain

$$(B.24) \quad 0 = \frac{(u_j^*)_i}{|(u_j^*)_i|} \left(|(u_j^*)_i| - (\sqrt{d_j})_i \right) + (\Lambda_j^*)_i.$$

On the other hand, when $(u_j^*)_i = 0$ for some index i , we have $(u_j^{t_{k_\ell}})_i \in B_r((u_j^*)_i) \setminus \{(u_j^*)_i\}$ to be nonzero. Taking the absolute value of (B.23) gives us

$$\left| (\Lambda_j^{t_{k_\ell}})_i + \beta_1 \left((u_j^{t_{k_\ell}+1})_i - (\mathcal{F}(\omega^{t_{k_\ell}} \circ S_j z^{k_\ell}))_i \right) \right| = \left| (u_j^{t_{k_\ell}+1})_i - (\sqrt{d_j})_i \right|.$$

Again, by (B.12) and (B.20), taking the limit yields

$$|(\Lambda_j^*)_i| = |(\sqrt{d_j})_i|,$$

which implies that there exists $u' \in \{u \in \mathbb{C} : |u| \leq 1\}$ such that $-u'(\sqrt{d_j})_i + (\Lambda_j^*)_i = 0$. This result and (B.24) give us (4.1a) for the AGM case. As for the IPM case, because $\lim_{x \rightarrow 0^+} x - d \log x = +\infty$, it follows that $(u_j^*)_i \neq 0$ for all i , so we only need to worry about the nonzero case. Hence, verifying (4.1a) for IPM requires computation similar to the nonzero case for AGM, so it is omitted for brevity.

At iteration t_{k_ℓ} , the first-order optimality condition of (3.6c) is

$$(B.25) \quad -\frac{y^{t_{k_\ell}}}{\lambda} - \frac{\beta_2}{\lambda} (v^{t_{k_\ell}} - \nabla z^{t_{k_\ell}}) \in \partial (\|v^{t_{k_\ell}+1}\|_1 - \alpha \|v^{t_{k_\ell}+1}\|_{2,1}).$$

By (B.13) and (B.21), we have

$$\begin{aligned} \lim_{\ell \rightarrow \infty} -\frac{y^{t_{k_\ell}}}{\lambda} - \frac{\beta_2}{\lambda} (v^{t_{k_\ell}} - \nabla z^{t_{k_\ell}}) &= -\frac{y^*}{\lambda}, \\ \lim_{\ell \rightarrow \infty} v^{t_{k_\ell}+1} &= \lim_{\ell \rightarrow \infty} v^{t_{k_\ell}} = v^*. \end{aligned}$$

By continuity, $\lim_{\ell \rightarrow \infty} \|v^{t_{k_\ell}+1}\|_1 - \alpha \|v^{t_{k_\ell}+1}\|_{2,1} = \|v^*\|_1 - \alpha \|v^*\|_{2,1}$. Altogether, by closedness of limiting subdifferential, we establish (4.1b).

Lastly, we prove (4.1e')-(4.1f'). At iteration t_{k_ℓ} , we have

$$\nabla_\omega \mathcal{L}(\omega^{t_{k_\ell}}) = - \sum_{j=1}^N \left\{ \beta_1 (S_j z^{t_{k_\ell}})^* \circ \left[\mathcal{F}^{-1} \left(u_j^{t_{k_\ell}+1} + \frac{\Lambda_j^{t_{k_\ell}}}{\beta_1} \right) - \omega^{t_{k_\ell}} \circ S_j z^{t_{k_\ell}} \right] \right\}.$$

Taking the limit, we see that

$$\nabla_\omega \mathcal{L}(Z^*, \Omega^*) = - \sum_{j=1}^N \left\{ \beta_1 (S_j z^*)^* \circ \left[\mathcal{F}^{-1} \left(u_j^* + \frac{\Lambda_j^*}{\beta_1} \right) - \omega^* \circ S_j z^* \right] \right\} = \lim_{\ell \rightarrow \infty} \nabla_\omega \mathcal{L}(\omega^{t_{k_\ell}}).$$

Applying Fatou's Lemma to (B.16), we have $\mathbb{E} [\|\nabla_\omega \mathcal{L}(Z^*, \Omega^*)\|_2^2] \leq \liminf_{\ell \rightarrow \infty} \mathbb{E} [\|\nabla_\omega \mathcal{L}(\omega^{t_{k_\ell}})\|_2^2] = 0$. Proving (4.1f') is similar to proving (4.1e'), so we omit the proof. Altogether, (Z^*, Ω^*) is a stochastic KKT point a.s. ■

REFERENCES

- [1] H. H. BAUSCHKE, P. L. COMBETTES, AND D. R. LUKE, *Hybrid projection–reflection method for phase retrieval*, Journal of the Optical Society of America A, 20 (2003), pp. 1025–1034.
- [2] J. BOLTE, S. SABACH, AND M. TEBoulLE, *Proximal alternating linearized minimization for nonconvex and nonsmooth problems*, Mathematical Programming, 146 (2014), pp. 459–494.
- [3] L. BOTTOU, F. E. CURTIS, AND J. NOCEDAL, *Optimization methods for large-scale machine learning*, SIAM Review, 60 (2018), pp. 223–311.
- [4] S. BOYD, N. PARIKH, AND E. CHU, *Distributed optimization and statistical learning via the alternating direction method of multipliers*, Now Publishers Inc, 2011.
- [5] K. BUI, F. PARK, Y. LOU, AND J. XIN, *A weighted difference of anisotropic and isotropic total variation for relaxed Mumford–Shah color and multiphase image segmentation*, SIAM Journal on Imaging Sciences, 14 (2021), pp. 1078–1113.
- [6] E. J. CANDÈS, X. LI, AND M. SOLTANOLKOTABI, *Phase retrieval via Wirtinger flow: Theory and algorithms*, IEEE Transactions on Information Theory, 61 (2015), pp. 1985–2007.
- [7] E. J. CANDÈS, T. STROHMER, AND V. VORONINSKI, *PhaseLift: Exact and stable signal recovery from magnitude measurements via convex programming*, Communications on Pure and Applied Mathematics, 66 (2013), pp. 1241–1274.
- [8] H. CHANG, P. ENFEDAQUE, AND S. MARCHESINI, *Blind ptychographic phase retrieval via convergent alternating direction method of multipliers*, SIAM Journal on Imaging Sciences, 12 (2019), pp. 153–185.
- [9] H. CHANG, R. GLOWINSKI, S. MARCHESINI, X.-C. TAI, Y. WANG, AND T. ZENG, *Overlapping domain decomposition methods for ptychographic imaging*, SIAM Journal on Scientific Computing, 43 (2021), pp. B570–B597.
- [10] H. CHANG, Y. LOU, Y. DUAN, AND S. MARCHESINI, *Total variation–based phase retrieval for Poisson noise removal*, SIAM Journal on Imaging Sciences, 11 (2018), pp. 24–55.
- [11] H. CHANG, Y. LOU, M. K. NG, AND T. ZENG, *Phase retrieval from incomplete magnitude information via total variation regularization*, SIAM Journal on Scientific Computing, 38 (2016), pp. A3672–A3695.
- [12] H. CHANG, S. MARCHESINI, Y. LOU, AND T. ZENG, *Variational phase retrieval with globally convergent preconditioned proximal algorithm*, SIAM Journal on Imaging Sciences, 11 (2018), pp. 56–93.
- [13] Y. CHEN AND E. J. CANDÈS, *Solving random quadratic systems of equations is nearly as easy as solving linear systems*, Communications on Pure and Applied Mathematics, 70 (2017), pp. 822–883.
- [14] L. DE CARO, D. ALTAMURA, M. ARCINIEGAS, D. SILIQI, M. R. KIM, T. SIBILLANO, L. MANNA, AND C. GIANNINI, *Ptychographic imaging of branched colloidal nanocrystals embedded in free-standing thick polystyrene films*, Scientific Reports, 6 (2016), pp. 1–8.
- [15] P. ENFEDAQUE, H. CHANG, B. ENDERS, D. SHAPIRO, AND S. MARCHESINI, *High performance partial coherent x-ray ptychography*, in International Conference on Computational Science, Springer, 2019, pp. 46–59.
- [16] S. ESEDOĞLU AND S. J. OSHER, *Decomposition of images by the anisotropic Rudin–Osher–Fatemi model*, Communications on Pure and Applied Mathematics, 57 (2004), pp. 1609–1626.
- [17] A. FANNJIANG AND T. STROHMER, *The numerics of phase retrieval*, Acta Numerica, 29 (2020), pp. 125–228.
- [18] P. GOYAL, P. DOLLÁR, R. GIRSHICK, P. NOORDHUIS, L. WESOŁOWSKI, A. KYROLA, A. TULLOCH, Y. JIA, AND K. HE, *Accurate, large minibatch SGD: Training Imagenet in 1 hour*, arXiv preprint arXiv:1706.02677, (2017).
- [19] A. GREENBAUM, *Behavior of slightly perturbed lanczos and conjugate-gradient recurrences*, Linear Algebra and its Applications, 113 (1989), pp. 7–63.
- [20] K. HE, X. ZHANG, S. REN, AND J. SUN, *Deep residual learning for image recognition*, in Proceedings of the IEEE conference on computer vision and pattern recognition, 2016, pp. 770–778.
- [21] R. HESSE, D. R. LUKE, S. SABACH, AND M. K. TAM, *Proximal heterogeneous block implicit-explicit method and application to blind ptychographic diffraction imaging*, SIAM Journal on Imaging Sciences, 8 (2015), pp. 426–457.
- [22] M. R. HESTENES AND E. STIEFEL, *Methods of conjugate gradients for solving*, Journal of research of the National Bureau of Standards, 49 (1952), p. 409.

- [23] R. JOHNSON AND T. ZHANG, *Accelerating stochastic gradient descent using predictive variance reduction*, Advances in neural information processing systems, 26 (2013), pp. 315–323.
- [24] Y.-F. KE AND C.-F. MA, *Alternating direction methods for solving a class of sylvester-like matrix equations*, Linear and Multilinear Algebra, 65 (2017), pp. 2268–2292.
- [25] H. LIU, K. DENG, H. LIU, AND Z. WEN, *An entropy-regularized admm for binary quadratic programming*, Journal of Global Optimization, (2022), pp. 1–33.
- [26] Q. LIU, X. SHEN, AND Y. GU, *Linearized admm for nonconvex nonsmooth optimization with convergence analysis*, IEEE Access, 7 (2019), pp. 76131–76144.
- [27] Y. LOU AND M. YAN, *Fast L_1 - L_2 minimization via a proximal operator*, Journal of Scientific Computing, 74 (2018), pp. 767–785.
- [28] Y. LOU, P. YIN, Q. HE, AND J. XIN, *Computing sparse representation in a highly coherent dictionary based on difference of L_1 and L_2* , Journal of Scientific Computing, 64 (2015), pp. 178–196.
- [29] Y. LOU, P. YIN, AND J. XIN, *Point source super-resolution via non-convex L_1 based methods*, Journal of Scientific Computing, 68 (2016), pp. 1082–1100.
- [30] Y. LOU, T. ZENG, S. OSHER, AND J. XIN, *A weighted difference of anisotropic and isotropic total variation model for image processing*, SIAM Journal on Imaging Sciences, 8 (2015), pp. 1798–1823.
- [31] D. R. LUKE, *Relaxed averaged alternating reflections for diffraction imaging*, Inverse Problems, 21 (2004), p. 37.
- [32] A. MAIDEN, D. JOHNSON, AND P. LI, *Further improvements to the ptychographical iterative engine*, Optica, 4 (2017), pp. 736–745.
- [33] A. M. MAIDEN AND J. M. RODENBURG, *An improved ptychographical phase retrieval algorithm for diffractive imaging*, Ultramicroscopy, 109 (2009), pp. 1256–1262.
- [34] J. MARRISON, L. RÄTY, P. MARRIOTT, AND P. O’TOOLE, *Ptychography—a label free, high-contrast imaging technique for live cells using quantitative phase information*, Scientific Reports, 3 (2013), pp. 1–7.
- [35] Y. S. NASHED, D. J. VINE, T. PETERKA, J. DENG, R. ROSS, AND C. JACOBSEN, *Parallel ptychographic reconstruction*, Optics Express, 22 (2014), pp. 32082–32097.
- [36] L. M. NGUYEN, J. LIU, K. SCHEINBERG, AND M. TAKÁČ, *Sarah: A novel method for machine learning problems using stochastic recursive gradient*, in International Conference on Machine Learning, PMLR, 2017, pp. 2613–2621.
- [37] Y. OUYANG, Y. CHEN, G. LAN, AND E. PASILIAO JR, *An accelerated linearized alternating direction method of multipliers*, SIAM Journal on Imaging Sciences, 8 (2015), pp. 644–681.
- [38] F. PARK, Y. LOU, AND J. XIN, *A weighted difference of anisotropic and isotropic total variation for relaxed mumford-shah image segmentation*, in 2016 IEEE International Conference on Image Processing (ICIP), IEEE, 2016, pp. 4314–4318.
- [39] M. PHAM, A. RANA, J. MIAO, AND S. OSHER, *Semi-implicit relaxed Douglas-Rachford algorithm (sDR) for ptychography*, Optics Express, 27 (2019), pp. 31246–31260.
- [40] H. ROBBINS AND S. MONRO, *A stochastic approximation method*, The annals of mathematical statistics, (1951), pp. 400–407.
- [41] R. T. ROCKAFELLAR AND R. J.-B. WETS, *Variational analysis*, vol. 317, Springer Science & Business Media, 2009.
- [42] J. M. RODENBURG AND H. M. FAULKNER, *A phase retrieval algorithm for shifting illumination*, Applied Physics Letters, 85 (2004), pp. 4795–4797.
- [43] L. I. RUDIN, S. OSHER, AND E. FATEMI, *Nonlinear total variation based noise removal algorithms*, Physica D: nonlinear phenomena, 60 (1992), pp. 259–268.
- [44] Y. SHECHTMAN, Y. C. ELDAR, O. COHEN, H. N. CHAPMAN, J. MIAO, AND M. SEGEV, *Phase retrieval with application to optical imaging: a contemporary overview*, IEEE signal processing magazine, 32 (2015), pp. 87–109.
- [45] A. SUZUKI, K. SHIMOMURA, M. HIROSE, N. BURDET, AND Y. TAKAHASHI, *Dark-field x-ray ptychography: Towards high-resolution imaging of thick and unstained biological specimens*, Scientific Reports, 6 (2016), pp. 1–9.
- [46] P. THIBAUT, M. DIEROLF, O. BUNK, A. MENZEL, AND F. PFEIFFER, *Probe retrieval in ptychographic coherent diffractive imaging*, Ultramicroscopy, 109 (2009), pp. 338–343.
- [47] I. WALDSPURGER, A. D’ASPREMONT, AND S. MALLAT, *Phase recovery, maxcut and complex semidefinite*

- programming*, Mathematical Programming, 149 (2015), pp. 47–81.
- [48] A. WALTHER, *The question of phase retrieval in optics*, Optica Acta: International Journal of Optics, 10 (1963), pp. 41–49.
 - [49] Y. WANG, W. YIN, AND J. ZENG, *Global convergence of admm in nonconvex nonsmooth optimization*, Journal of Scientific Computing, 78 (2019), pp. 29–63.
 - [50] Z. WANG, A. C. BOVIK, H. R. SHEIKH, AND E. P. SIMONCELLI, *Image quality assessment: from error visibility to structural similarity*, IEEE transactions on image processing, 13 (2004), pp. 600–612.
 - [51] Z. WEN, C. YANG, X. LIU, AND S. MARCHESINI, *Alternating direction methods for classical and ptychographic phase retrieval*, Inverse Problems, 28 (2012), p. 115010.
 - [52] S. WU FUNG AND Z. DI, *Multigrid optimization for large-scale ptychographic phase retrieval*, SIAM Journal on Imaging Sciences, 13 (2020), pp. 214–233.
 - [53] Y. XU, W. YIN, Z. WEN, AND Y. ZHANG, *An alternating direction algorithm for matrix completion with nonnegative factors*, Frontiers of Mathematics in China, 7 (2012), pp. 365–384.
 - [54] P. YIN, Y. LOU, Q. HE, AND J. XIN, *Minimization of ℓ_{1-2} for compressed sensing*, SIAM Journal on Scientific Computing, 37 (2015), pp. A536–A563.
 - [55] P. YIN AND J. XIN, *PhaseLiftOff: an accurate and stable phase retrieval method based on difference of trace and frobenius norms*, Communications in Mathematical Sciences, 13 (2014), pp. 1033–1049.
 - [56] Z. YUAN, H. WANG, AND Q. WANG, *Phase retrieval via sparse Wirtinger flow*, Journal of Computational and Applied Mathematics, 355 (2019), pp. 162–173.
 - [57] H. ZHANG, Y. ZHOU, Y. LIANG, AND Y. CHI, *A nonconvex approach for phase retrieval: Reshaped Wirtinger flow and incremental algorithms*, Journal of Machine Learning Research, 18 (2017).
 - [58] L. ZHOU, J. SONG, J. S. KIM, X. PEI, C. HUANG, M. BOYCE, L. MENDONÇA, D. CLARE, A. SIEBERT, C. S. ALLEN, ET AL., *Low-dose phase retrieval of biological specimens using cryo-electron ptychography*, Nature Communications, 11 (2020), pp. 1–9.